# Induced 2C Expression and Implantation-Competent Blastocyst-like Cysts from Primed Pluripotent Stem Cells

AUTHOR(S):

Kime, Cody; Kiyonari, Hiroshi; Ohtsuka, Satoshi; Kohbayashi, Eiko; Asahi, Michio; Yamanaka, Shinya; Takahashi, Masayo; Tomoda, Kiichiro

CITATION:

Kime, Cody ...[et al]. Induced 2C Expression and Implantation-Competent Blastocyst-like Cysts from Primed Pluripotent Stem Cells. Stem Cell Reports 2019, 13(3): 485-498

ISSUE DATE:

2019-09-10

URL:

http://hdl.handle.net/2433/255122

Stem Cell Reports
Article
ISSCR
OPEN ACCESS

# Induced 2C Expression and Implantation-Competent Blastocyst-like Cysts from Primed Pluripotent Stem Cells

Cody Kime,[1,2,*] Hiroshi Kiyonari,[3] Satoshi Ohtsuka,[4] Eiko Kohbayashi,[5] Michio Asahi,[6] Shinya Yamanaka,[1,7] Masayo Takahashi,[2] and Kiichiro Tomoda[1,6,*]

[1]Gladstone Institute of Cardiovascular Disease, San Francisco, CA 94158, USA
[2]Lab of Retinal Regeneration, RIKEN Center for Biosystems Dynamics Research, Kobe 650-0047, Japan
[3]Laboratory for Animal Resources and Genetic Engineering, RIKEN Center for Biosystems Dynamics Research, Kobe 650-0047, Japan
[4]Department of Life Science, Medical Research Institute, Kanazawa Medical University, Ishikawa 920-0293, Japan
[5]Second Department of Internal Medicine, Osaka Medical College, Osaka 569-8686, Japan
[6]Department of Pharmacology, Faculty of Medicine, Osaka Medical College, Osaka 569-8686, Japan
[7]Center for iPS Cell Research and Application (CiRA), Kyoto University, Kyoto 606-8507, Japan
*Correspondence: cody.kime@riken.jp (C.K.), pha050@osaka-med.ac.jp (K.T.)
https://doi.org/10.1016/j.stemcr.2019.07.011

## SUMMARY

Soon after fertilization, the few totipotent cells of mammalian embryos diverge to form a structure called the blastocyst (BC). Although numerous cell types, including germ cells and extended-pluripotency stem cells, have been developed from pluripotent stem cells (PSCs) *in vitro*, generating functional BCs only from PSCs remains elusive. Here, we describe induced self-organizing 3D BC-like cysts (iBLCs) generated from mouse PSC culture. Resembling natural BCs, iBLCs have a blastocoel-like cavity and were formed with outer cells expressing trophectoderm lineage markers and with inner cells expressing pluripotency markers. iBLCs transplanted to pseudopregnant mice uteruses implanted, induced decidualization, and exhibited growth and development before resorption, demonstrating that iBLCs are implantation competent. iBLC precursor intermediates required the transcription factor Prdm14 and concomitantly activated the totipotency-related cleavage-stage MERVL reporter and 2C genes. Thus, our system may contribute to the understanding of molecular mechanisms underpinning totipotency, embryogenesis, and implantation.

## INTRODUCTION

During early mammalian development, a fertilized egg (zygote) completely intersects the animal life cycle upon zygotic genome activation (ZGA), the event whereby gamete totipotent genomes of the pronucleus are epigenetically activated and rapidly enter cleavage (Seydoux and Braun, 2006; Wu et al., 2017). The zygote cleaves and later polarizes as symmetry bifurcates to form the blastocyst (BC) with emerging trophoblasts and pluripotent cells of the inner cell mass (ICM) (Hirate et al., 2015; Nishioka et al., 2009; Stephenson et al., 2010; Yu et al., 2016). The ICM further differentiates to the embryonic epiblast and primitive endoderm (PrE) while preparing for implantation (Guo et al., 2010; Plusa et al., 2008; Saiz and Plusa, 2013). BC implantation is crucial to natural development and is tightly regulated at several molecular and cellular levels that must occur in a short developmental window: failed implantation is a major cause of early pregnancy loss (Cha et al., 2012; Norwitz et al., 2001). Defective embryos can also fail later and begin resorption (Cossée et al., 2000; Flores et al., 2014).

The zygote and cleavage stages exhibit true totipotency, isogenically preceding all extraembryonic (ExEm, vegetal) and embryonic (Em, animal) cell bidirectional development toward entire organisms. From plant tissue cultures, specific cytokine, vitamin, and plant hormone (auxins) ratios are adjusted to induce totipotent transient cells for propagating isogenic embryos (Steward et al., 1958). In mammals, isogenic 3D BCs from differentiated cells are both attractive and elusive, and experiments inducing implantation-competent isogenic BCs entirely from pluripotent stem cells (PSCs) are unprecedented.

In PSC reprogramming and conversion experiments with specific cytokines, nutrient, and lipid (Kime et al., 2016), we observed cell organization and hemispherical cysts with features of BCs. Thereafter we developed a system to induce 8–16 cell iBLC precursors (iBLC-PCs) that self-organized into BC-like cysts *in vitro*, termed iBLCs. iBLC-PCs were found to be *Prdm14*-dependent and concomitantly expressed the murine endogenous retrovirus (*MERVL*) live 2C-state reporter, which suggested ZGA mechanisms related to *Zscan4* expression (Macfarlan et al., 2012; Wu et al., 2017). Analysis of YAP (Yes-associated protein) in iBLC-PCs and early iBLCs revealed a transition from a non-polarized state to a polarized cyst, closely resembling early pre-implantation embryogenesis (Bedzhov et al., 2014; Nishioka et al., 2009; Stephenson et al., 2010).

iBLCs were implantation competent and induced focal decidualization in the uterus that recruited surrogate blood supply and expanded the embryonic cavity. Implanted iBLCs could grow and produce many cell types like implanted embryos, but eventually failed in embryonic resorption. We anticipate that this system may lead to

simplified isogenic embryo production for research, medicine, and uncovering the intricacies of totipotency and implantation.

## RESULTS

### Defined Conditions Generate Early Embryo-like Tissues

*In vitro* pluripotency is characterized in two distinct states: a pre-implantation BC ICM-like state (naive) and a post-implantation epiblast-like state (primed). Naive female PSCs have two active X chromosomes (Xa/Xa), and primed female PSCs have inactivated one of those X chromosomes (Xa/Xi) (Payer et al., 2011). We employed a primed female mouse epiblast stem cell (mEpiSC) line with a constitutive green fluorescent protein transgene on the Xi chromosome (XGFP). XGFP is silent in the mEpiSCs and is expressed upon Xi reactivation to Xa, a sophisticated epigenetic reprogramming hallmark of naive pluripotency, the ICM, and often of cleavage-stage totipotent cells (Bao et al., 2009; Kime et al., 2016; Monk and Harper, 1979; Okamoto et al., 2004).

Under our defined conditions we greatly enhanced cell reprogramming, and robust primed- to naive-state PSC conversion experiments (Kime et al., 2016) also produced BC-like hemispheres and structures resembling early embryonic material among rapid X chromosome reactivation, reported here. The hemispheres had BC-like organization with important cell-lineage markers for trophoblasts, embryonic, and PrE cells (Figures S1 and S2; Video S1); we previously reported the embryonic potency of the XGFP$^+$ cells(Kime et al., 2016). We observed NANOG$^+$XGFP$^+$ ICM-like cells with no bright DNA-stain puncta, which may indicate the loss of heterochromatin usually found in a rare transient Zscan4$^+$ 2C-like state (Akiyama et al., 2015; Wu et al., 2016) (Figure S1A). The outer cells and cells of the inner face of the ICM-like mass were negative for XGFP and positive for TROMA-I, an ExEm lineage marker. We examined important PrE markers and found GATA4 enriched cells that were XGFP-negative and platelet-derived growth factor receptor A (PDGFRa)-positive co-localized at the inner face to resemble the hypoblast of hatching BCs (Figures S1D and S1E) (Plusa et al., 2008). GATA6, a PrE gene regulated alongside GATA4 (Figure S1D) (Morgani and Brickman, 2015; Plusa et al., 2008; Saiz and Plusa, 2013), was expressed among a population positioned similar to the GATA4$^+$/PDGFRa$^+$ cells(Figures S1D–S1F) (Guo et al., 2010; Morgani and Brickman, 2015; Plusa et al., 2008). Taken together, the BC-like hemispheres reflected the intricate regulation of X chromosome activity, gene expression, and cell organization of BCs including PrE formation. As such, the possibility that all embryonic cell lineages were induced inspired us to consider that transient total potential might be installed in some converting cells.

Such primed-to-naive-state conversions strongly induced Prdm and Id family genes that broadly regulate the genome and are curiously related to the cleavage stage, early embryo, and germline preparation (Figure S2B) (Burton et al., 2013; Hiller et al., 2010; Luna-Zurita and Bruneau, 2013; Yamaji et al., 2008; Yang et al., 2017). Within this reprogramming context, we tested the SMAD2/3 signaling ALK5 inhibitor SB431542 that inhibits primed state ActivinA/TGFβ (transforming growth factor β) signaling and is described for *in vitro* germ-cell differentiation (Chen et al., 2012). The cultures released floating small cell clusters and cysts that we speculated could have BC-like properties similar to the related BC-like hemispheres. We then optimized phase-1 and -2 treatments of defined conditions (Figure 1A), which produced 5–30 floating BC-like cysts by day 7 (Figure S3A and Table S1). The BC-like cysts stuck together as they grew to resemble hatched BCs on day 8, so for most experiments we qualitatively assessed and isolated them on day 7 based on morphological similarity to early BCs (e.g., appropriate size, neatly round, trophectoderm (TE)-like outer cells, a putative ICM; Figure 1B). DNA staining of the cysts revealed a compact ICM-like mass and large flat TE-like cells surrounding the possible blastocoel (Figure S3B).

To explore the origin of the BC-like cysts, we individually cultured the small clusters that appeared nonpolar on day 5.5 (Figure 1C, left panel). Some clusters (usually ~5%–50%) grew, changed morphology, and formed a blastocoel-like cavity as a cyst with BC-like morphology (Figure 1C). From these findings and the investigation described hereafter, we termed the day-7 floating structures "induced blastocyst-like cysts" (iBLCs) that grew, polarized, and self-organized from small cell clusters as iBLC precursors (iBLC-PCs).

### iBLC-PCs Involve Early Embryonic Genes

BCs develop from a totipotent state. To gain molecular insights into iBLC induction, we prepared XGFP mEpiSC with the well-studied 2C *MERVL* live totipotency-related reporter (*MERVL*::RFP, Figure S3C) (Macfarlan et al., 2012; Wu et al., 2017), which was undetectable in all mEpiSCs as expected. On days 5–6 of iBLC induction, we observed RFP expression in some of the characteristic loci where iBLC-PCs emerge, and some RFP$^+$ cells also expressed XGFP, perhaps consistent with Xa/Xa status of cleavage-stage embryos (Figure 2A) (Okamoto et al., 2004). Many iBLC-PCs were composed of several cells concurrently expressing *MERVL*::RFP (Figure 2B). In many cases, the RFP expression was weaker in the iBLC-PCs than in cells on the plate and XGFP was usually undetectable, suggesting that both reporters might be downregulated similarly to

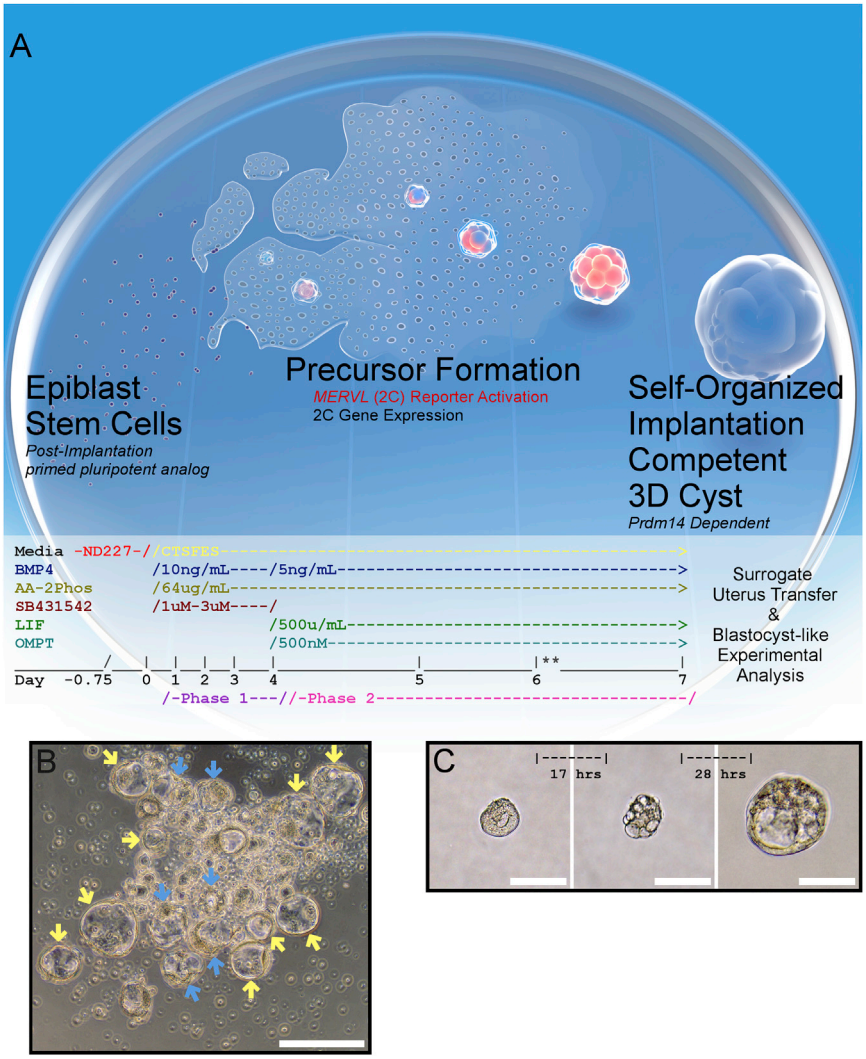


**Figure 1. Defined Conditions Induce Early Embryo-like Structures from Primed PSCs**

(A) iBLC System Overview: Typically, ~40,000 primed mEpiSCs are plated and induced to *MERVL*::RFP$^+$ cell cluster precursors (iBLC-PC) that differentiate into ~5–30 BC-like cysts (iBLCs). Two-phase iBLC induction media timing to induce mEpiSC to iBLCs. **Supernatant iBLC-PCs are collected to ultralow attachment (ULA) wells on day 6, and high-quality BC-like iBLCs are selected on day 7 by embryo pipette.

(B) iBLCs are qualified with BC-like characteristics (yellow arrows) or excluded (blue arrows) after pooling ULA plate for downstream experiments. Scale bar, 200 μm.

(C) Isolated iBLC-PC developing into iBLC over time. Scale bars, 100 μm.

what is observed in compacting early embryos. Notably, RFP signals were further reduced in emergent iBLCs (Figure 2C) and, after iBLC-PC harvest, RFP$^+$ cells with or without XGFP expression were variably maintained on iBLC generation plates for several days in phase-2 medium.

To investigate the implications of the 2C *MERVL*::RFP reporter in our system, we pooled RFP$^+$ or RFP$^-$ cell clusters resembling iBLC-PCs on day 6 and examined early embryonic gene expression. We found that only *MERVL*::RFP$^+$ iBLC-PCs induced *Zscan4* and *Tsctv3*, both critically important 2C markers (Falco et al., 2007; Macfarlan et al., 2011, 2012), and with high relative expression (Figures 2D and S3D). These results validated that the 2C *MERVL*::*RFP* reporter represented a meaningful unique 2C-like gene expression in iBLC-PCs.

Next, we focused on *Prdm14*, a critical transcription factor shared in the germline and early embryo (Hackett et al., 2017; Nakaki and Saitou, 2014). *Prdm14* was very low or undetectable in mEpiSCs yet could be induced in early iBLCs (Figure 2E). Consistent with these data, constitutive short hairpin RNA against *Prdm14* (*Prdm14* knockdown [KD]) did not have noticeable effects on mEpiSCs or in the first 5 days of iBLC generation (Figure 2G). However, on day 6 with efficient *Prdm14* KD (Figure 2F), iBLC-PCs were nearly completely aborted and many peripheral cells of typical iBLC-PC loci degraded (Figure 2G), and supernatants did not generate iBLCs. We were curious as to whether the 2C marker *Zscan4* would be lost from degrading cells, yet *Prdm14* KD insignificantly but variably affected the induction of *Zscan4* in the population while permitting consistently higher *Zfp42* (Rex1) expression (Figure 2F). Collectively, these results suggest that a 2C-like state is induced in a population wherein iBLC-PC/iBLC survival may be *Prdm14* dependent.

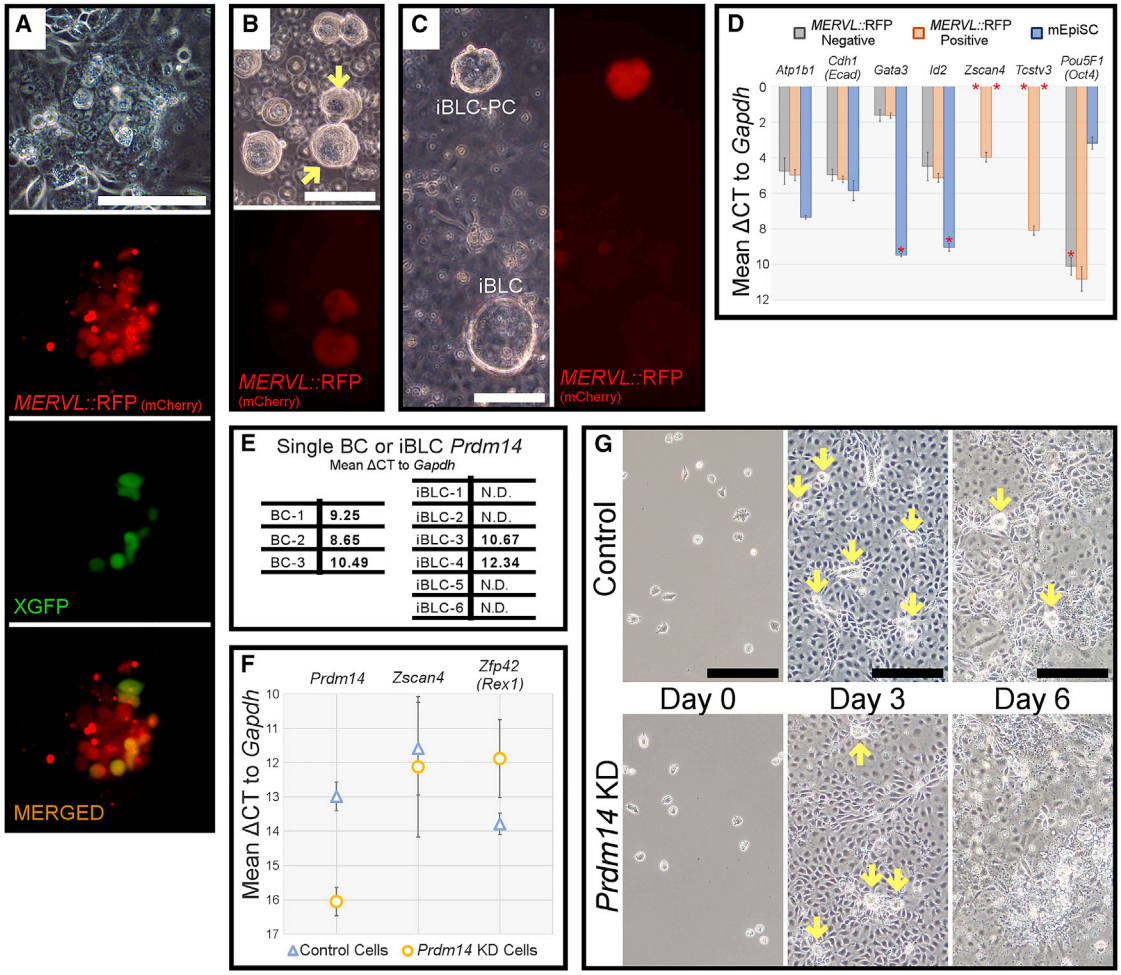


**Figure 2. iBLC Generation Activates 2C MERVL Reporter in iBLC-PCs and Requires Prdm14**

(A) iBLC system day 6 co-localized expression of *MERVL*::RFP and XGFP reporters. Scale bar, 100 μm.

(B) *MERVL*::RFP$^+$ iBLC-PCs (yellow arrows) in ULA plate on day 6. Scale bar, 100 μm.

(C) *MERVL*::RFP is expressed strongly in iBLC-PCs yet poorly in differentiating iBLC, observed on day 8. Scale bar, 100 μm.

(D) qRT-PCR of *MERVL*::RFP reporter-derived clusters on day 6, pooled by RFP$^-$ or RFP$^+$ expression; shown as mean ΔCt to *Gapdh*. mEpiSC prepared for qRT-PCR by the same means were used as control. Data represent biological triplicate samples tested in technical triplicate, and error bars represent standard deviation. Asterisks denote sample detection notes: *Gata3* detected in one mEpiSC sample, *Id2* detected in two mEpiSC samples, *Zscan4* not detected in RFP$^-$/mEpiSC samples, *Tcstv3* not detected in RFP$^-$/mEpiSC samples, *Pou5F1* (Oct4) detected in two RFP$^-$ samples.

(E) Single isolated BC and iBLC qRT-PCR for *Prdm14*.

(F) qRT-PCR of control and *Prdm14* KD cell plate cDNA samples for *Prdm14*, *Zscan4*, and *Zfp42* (Rex1) on day 6 of iBLC generation. Data represent biological triplicate samples tested in technical triplicate, and error bars represent standard deviation.

(G) Control and *Prdm14* KD mEpiSC are plated for iBLC induction. Loci that originate iBLC-PCs are initiated in both experiments by day 3 (yellow arrows). Control cells maintain iBLC-PCs through day 6 (yellow arrows) and *Prdm14* KD cells aborted iBLC-PCs. Scale bars, 200 μm.

## Induced Blastocyst-like Cysts Represent Pre-/Post-compacted Embryonic State

The transcription factor YAP governs positional information and polarization to bifurcate outer and inner cells during early embryonic development (Bedzhov et al., 2014; Nishioka et al., 2009). Thus, we examined cell positioning, along with YAP subcellular localization, in iBLC-PCs and iBLCs. Some iBLC-PCs resembled early embryos before compaction (Hirate et al., 2015; Nishioka et al., 2009; Yu et al., 2016) with morphologically homogeneous cells that equally expressed nuclear and cytosolic YAP (Figure 3A). Other iBLC-PCs implicated cell polarization with nuclear-enriched YAP among outer cells and nuclear-excluded YAP among inner cells (Figure 3B); emergent early

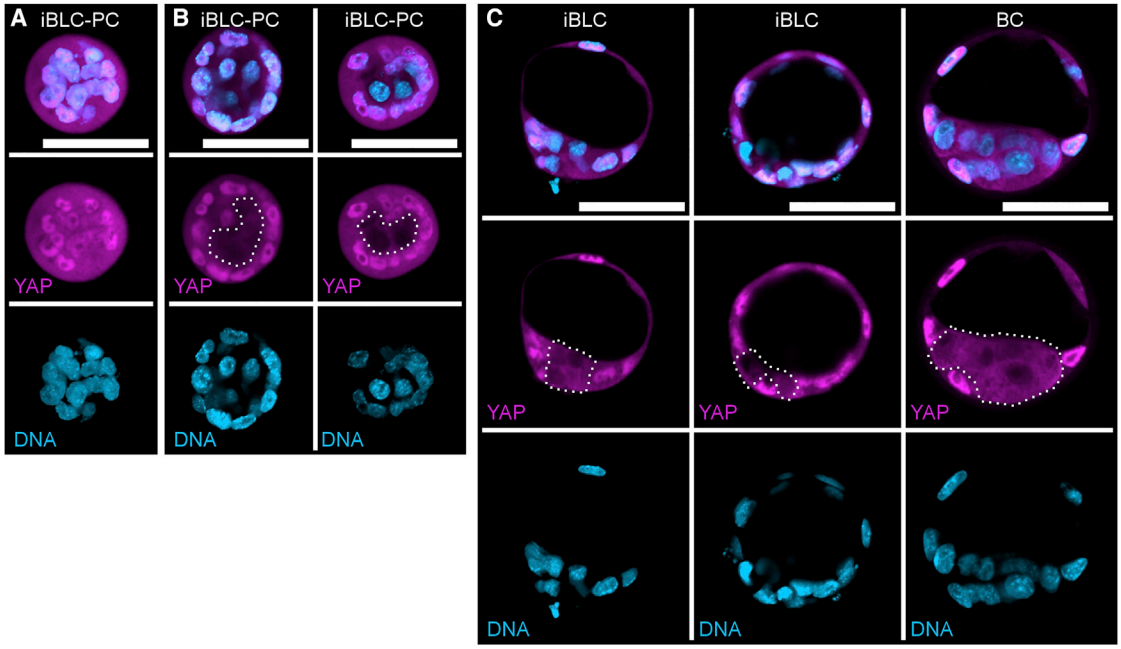


**Figure 3. iBLC-PCs and iBLCs May Follow Early Embryonic Polarization via YAP**

(A and B) iBLC-PCs stained for YAP (magenta) and DNA (light blue). Scale bars, 50 μm. Nuclear-excluded YAP region is outlined with dotted white line in (B).

(C) Early iBLCs and early BCs stained for YAP (magenta) and DNA (light blue). Scale bars, 50 μm. Nuclear-excluded YAP region is outlined with dotted white line.

iBLCs carried the same YAP pattern as early BCs (Figure 3C). Comprehensively, sample YAP expression resembled the developmental window where blastomeres polarize into compacting embryos and early BCs.

## iBLCs Express Important Genes but Lack Full BC Potency

Early BCs have an outer layer of trophoblast cells and an ICM of pluripotent cells without distinct PrE. Thus, BCs express genes important for inducing and developing both lineages. Gene expression analyses revealed individual early BCs and particularly individual early iBLCs had variations in expression, suggesting there is a difference in the quality, developmental timing, or both, in each sample; iBLC-3 had notably higher expression of several genes closer to that of BCs. The genes we checked that are first activated in totipotent cleavage-stage cells (e.g., *Atp1b1*, *Gata3*, *Id2*, *Zscan4*, *Bmp4*) were strongly upregulated in iBLCs to match detection in BCs. Remarkably, *Gata3* expression was high and even higher in iBLC-PC reprogramming samples (Figure 2D). Gata3 is expressed across early embryo development (Guo et al., 2010; Home et al., 2009) and was recently described as a master reprogramming factor that induced all three major *in vitro* cell culture equivalents of pre-implantation blastocysts (Benchetrit et al., 2019).

Genes involved in the outer cell-lineage development and/or function (e.g., *Atp1b1*, *Cdx2*, *Gata3*, and *Krt8* [Troma-I]) were strongly induced in iBLCs (Figure 4A and S3E), although *Cdx2* was usually much lower than in BCs. Critical pluripotent transcription factors *Nanog* and *Pou5f1* (Oct4) were also low in iBLCs but were still expressed among other pre-implantation pluripotency genes (e.g., *Tdgf1*, *Zfp42*) (Figures 4A and S3E). Collectively, outer/inner cell fate-specifying genes (e.g., *Cdx2*, *Eomes*, *Pou5F1* [Oct4]) were generally low in iBLCs (Figures 4A and S3E).

Low *Cdx2* and *Pou5f1* raised the question of whether iBLCs possess the TE-like outer and ICM-like mass. We also wondered whether iBLCs could regulate PrE genes as the cyst develops later. We examined detection and localization of CDX2, GATA3, OCT4, YAP, and the TE marker TROMA-I, in early iBLCs and early BCs by immunocytochemistry with well-characterized antibodies. For PrE regulation, we examined GATA4 and PDGFRa in early and late iBLCs to compare with early- and late-hatching BCs and previous reports (Guo et al., 2010; Plusa et al., 2008; Saiz and Plusa, 2013). The early iBLC inner cells downregulated CDX2, GATA3, and YAP like early BCs, although more extremely. GATA3 was found both cytosolic and nuclear in outer cells of both iBLCs and BCs while CDX2 in iBLC outer cells was mostly cytosolic and not enriched in

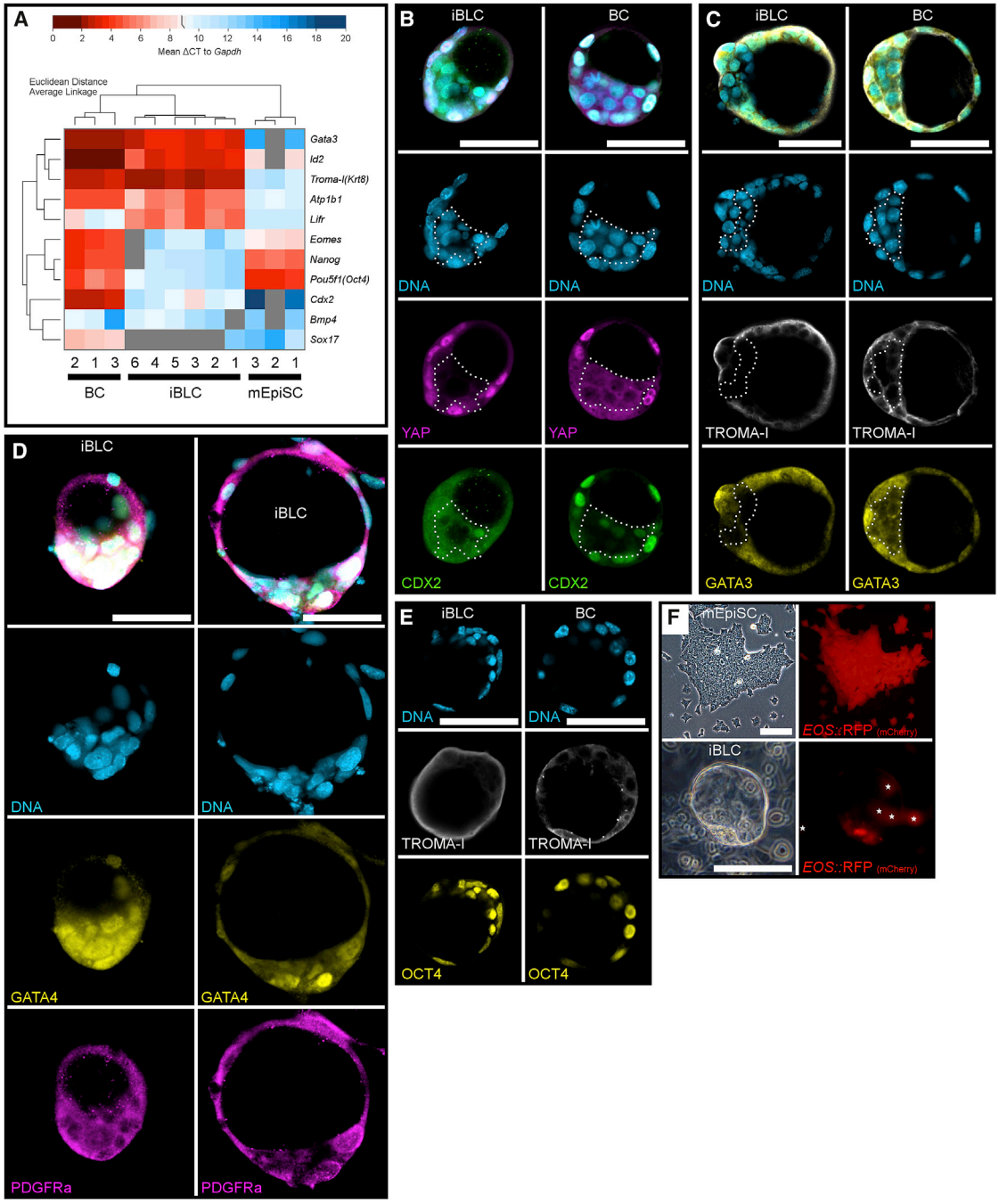


**Figure 4. iBLCs Share Many Characteristics with BCs**

(A) qRT-PCR of individual early BC, early iBLC, and mEpiSC colony cDNA samples, with Euclidean distance and clustering by average linkage, represented as a heatmap of global ΔCt to *Gapdh*.

(B) Early iBLC and early BC stained for DNA (light blue), YAP (magenta), and CDX2 (green). Nuclear-excluded YAP region is outlined with dotted white line. Scale bars, 50 μm.

(C) Early iBLC and early BC stained for DNA (light blue), TROMA-I (white), and GATA3 (yellow). Downregulated and nuclear-excluded GATA3 region is outlined with dotted white line. Scale bars, 50 μm.

(D) Early iBLC (left) and late iBLC (right) stained for DNA (light blue), GATA4 (yellow), and PDGFRa (magenta). Scale bars, 50 μm.

*(legend continued on next page)*

many nuclei (Figures 4B and 4C), suggesting poor CDX2 phosphorylation in iBLCs (Rings et al., 2001). PrE genes GATA4 and PDGFRa are expressed in all cells of the early embryo (Guo et al., 2010), and GATA4 protein was still detectable in all cells of early BCs and early iBLCs (Figure 4D, left; Figure S1D, top). Late-hatching BCs begin to neatly regulate nuclear GATA4 and membrane PDGFRa to a subset of mostly polar mass cells that collect and form the PrE hypoblast at the inner face of the ICM (Guo et al., 2010; Plusa et al., 2008); such PrE-like cell regulation was confirmed in hatching BCs and reflected in the BC-like hemispheres (Figures S1D and S1E). Our day-8 late iBLCs could also regulate GATA4 and PDGFRa to subsets of cells mostly at the ICM-like mass, although less neatly (Figures 4D and S3F). GATA4 enriched cells in late iBLCs collected together, similar to PrE hypoblast formation yet oddly different from BCs and our BC-like hemispheres (Figures S1D and S1E), because the putative iBLC PrE-like cells collected to the outer face of the ICM-like mass and were frequently observed bulging away from the iBLC main body (Figure S3F). Still, early iBLC outer cells strongly expressed TROMA-I, and iBLC inner cells better enriched nuclear OCT4 like early BCs (Figure 4E) (Bulut-Karslioglu et al., 2016; Ralston and Rossant, 2008). We anticipated protein detection differences and designed a qualitative semi-quantitative microscopy experiment that compared detector gain settings for iBLC and BC samples imaged on common microscopes with comparable stain, laser, and confocal settings (Supplemental Experimental Procedures). As expected, early iBLC OCT4 protein may have been lower because detection required higher microscope gain settings than BCs. Furthermore, TROMA-I protein was better detected in iBLCs than in BCs, consistent with the finding that *Krt8* (Troma-I) mRNAs were more highly expressed in iBLCs (Figures 4A–4E and S3E; Table S2).

To examine OCT4 and SOX2 functions we used the *EOS-S(4+)* live pluripotency reporter, which requires an OCT4/SOX2 heterodimer transcription activation. We cloned the reporter to drive red fluorescent proteins (*EOS*::RFP; Figure S3C and Experimental Procedures) and established *EOS*::RFP mEpiSCs that performed as expected (Hotta et al., 2009; Tomioka et al., 2002), with *EOS*::RFP$^+$ PSCs that lost RFP when differentiated (Figures 4F, S2C, and S3G). iBLCs generated from *EOS* reporter cells often exhibited RFP signals (Figure S3H) that were stronger in the iBLC putative ICM, suggesting that these cells may have functional OCT4/SOX2-driven *EOS*::RFP expression (Figure 4F).

Lastly, mouse embryonic stem cells (ESCs) and trophoblast stem cells (TSCs) can be established from BCs under different conditions. In ESC derivation conditions (Czechanski et al., 2014), outgrowths from isolated iBLCs and iBLC-PCs on feeder cells proliferated and expressed both XGFP and *EOS*::D2nRFP (Figure S4A and Experimental Procedures). These cells could be thereafter cultured comparable with naive ESCs in terms of colony morphologies and pluripotency gene expressions (Figures 5A, 5B, and S4A). We also derived colonies of slow-growing TE-like cells expressing CDX2 without *EOS* expression (Figure 5C). Attempts to derive TSCs in defined conditions (Latos and Hemberger, 2016; Ohinata and Tsukiyama, 2014) failed in part, but developed binucleated TPBPA$^+$ or PL-I$^+$ trophoblast giant cell (TGC)-like cells (Figure S4B).

## Reproducibility of iBLC Generation

Our various XGFP mEpiSC reporter sublines performed similarly throughout iBLC induction. Two published mEpiSC lines reacted similarly throughout and produced iBLCs with lower yields (Figure S4C) (Ohtsuka et al., 2012; Tesar et al., 2007). Another mEpiSC line with obvious cell culture characteristic differences failed completely (Parchem et al., 2014). Therefore, iBLC generation should be possible with many but not all mEpiSC lines.

## iBLCs Implant and Grow in Pseudopregnant Mice

The similarities between iBLCs and BCs led us to examine iBLC implantation and developmental potency *in utero*. We transferred BCs, iBLCs, mEpiSC clusters, and embryoid bodies (EBs) into separate uterus horns of sterile-male bred pseudopregnant mice; only BCs and iBLCs implanted and induced deciduae thereafter (Figures 6A and 6B). Deciduae from iBLC transfer were similar in focal morphology but often smaller than deciduae from BCs. Importantly, many iBLC deciduae recruited large maternal blood vessels seen in the uterus, and sectioning showed red brown color in the decidua basalis region, like natural deciduae (Figure 6B). iBLCs and BCs induced deciduae at 6.7% (10/149) and 69.2% (36/52), respectively (Figure 6A). We did not observe any deciduae from the mEpiSC cluster and EB controls.

Co-transferring control embryos that easily implant increases implantation rates of difficult embryos in assisted reproductive settings (Mochida et al., 2014). Co-transferring iBLCs with BCs frequently yielded more focal deciduae than the total number of BCs transferred (Table S3), suggesting that iBLCs implanted more efficiently. Also, co-transfer yields often had more deciduae than the estimated

(E) Early iBLC and early BC stained for DNA (light blue), TROMA-I (white), and OCT4 (yellow). Scale bars, 50 μm. Microscope gain settings from Table S2: Early iBLC DNA:398, TROMA-I:513, OCT4:731; Early BC DNA:363, TROMA-I:604, OCT4:601.
(F) *EOS*::RFP$^+$ mEpiSCs and late iBLCs above culture with *EOS*::RFP expression in the putative ICM. White stars label out-of-focus *EOS*::RFP$^+$ cells on the plate. Scale bars, 100 μm.

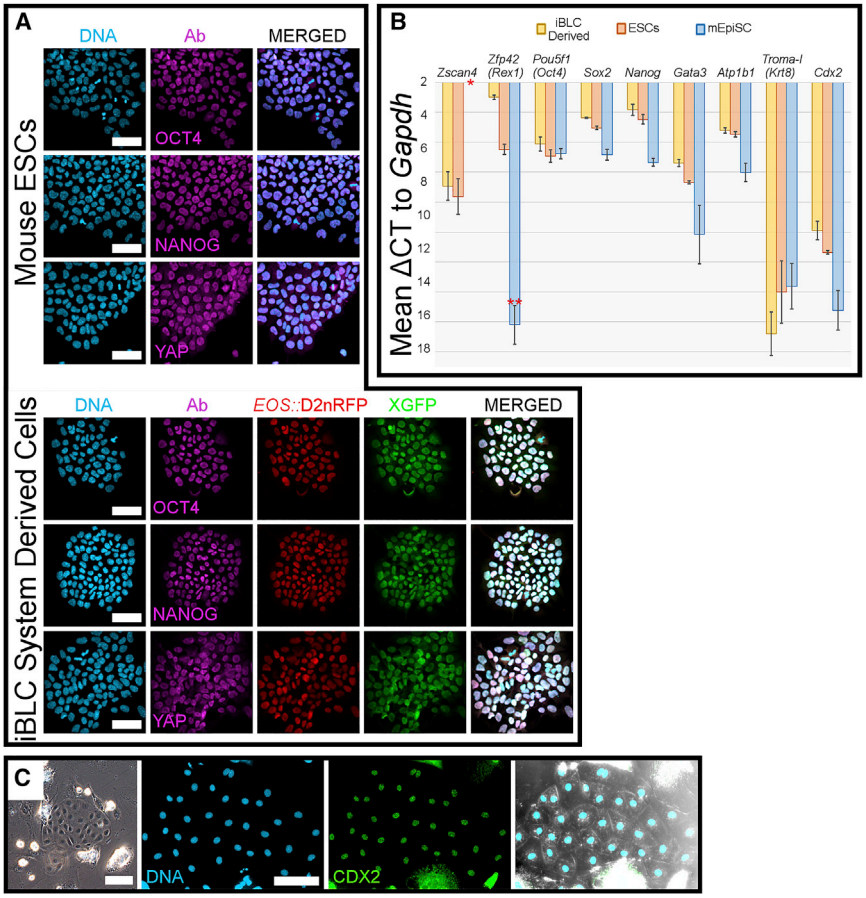


**Figure 5. iBLC System Outgrowths Generate Pluripotent and TE-Lineage Cells**

(A) Mouse ESCs and iBLC/iBLC-PC-derived ESC-like cells stained for OCT4, NANOG, or YAP (magenta), and DNA (light blue). iBLC/iBLC-PC-derived ES-like cells demonstrate X chromosome reactivation (XGFP$^+$) and express *EOS*::D2nRFP. Scale bars, 50 μm.

(B) qRT-PCR of mouse ESCs, iBLC/iBLC-PC-derived ES-like cells, and mEpiSC cDNA samples, shown as mean ΔCt to *Gapdh*. Data represent biological triplicate samples tested in technical triplicate, and error bars represent standard deviation. Asterisk indicates that *Zscan4* was not detected in mEpiSC; double asterisk indicates that *Zfp42* (Rex1) was detected in two mEpiSC samples.

(C) Left: live imaging of iBLC-derived TE-like cells. Right: TE-like cells stained for DNA (light blue) and CDX2 (green). Channels shown separately and merged. Scale bars, 100 μm.

sum based on BC-only and iBLC-only rates, suggesting that co-transfer increased iBLC or BC implantation, or both (Figure 6C and Table S3). Co-transferred mEpiSC clusters or EBs with BCs either inhibited or showed no improvement over estimated control BC implantation, highlighting the special ability of iBLCs (Figure 6C).

To confirm the origin of the deciduae from the iBLC experiments, we obtained genomic DNA from iBLC deciduae cryosections by laser capture microdissection (Figure S5A) and amplified a transgenic DNA region only in iBLCs (Figures S3C and 6D). This analysis confirmed that iBLC single-source and co-transfer experiments implanted to form deciduae with iBLC-derived tissue at the proper location for natural embryos. We therefore recognized that co-transferring BCs with iBLCs enhances the ability of iBLCs to implant and may prove more useful in later studies.

We performed hematoxylin and eosin (H&E) staining on cryosections of dissected deciduae from embryonic day 7.5 (E7.5) iBLC single-source transfer experiments (Figure 7). Like control deciduae (Figure S5B), iBLC-implanted deciduae were surrounded by uterine tissue and had distinct subregions; among which the decidua basalis showed vascular sinus foldings and red blood cells, confirming the maternal blood supply (Figures 7A, 7B, and S5B).

While iBLC-derived E7.5 tissues were larger than E6.5 control embryo tissues, many cells appeared pycnotic (Gardner and Johnson, 1972) and lacked a healthy appearance, and were collectively smaller than an E7.5 control embryo (Figures 7 and S5B). We also observed many blood mononuclear cells around the disfigured pycnotic tissues, indicating embryo resorption (Cossée et al., 2000; Flores et al., 2014) (Figures 7B and S5C). Nevertheless, careful examination of resorbing iBLC-derived tissues showed markedly diverse cell morphology and localization strikingly similar to findings of a previous report of natural resorbing embryos (Figures 7A and 7B) (Cossée et al., 2000). The sections had distinct disfigured tissues in the presumptive embryonic region with surrounding ExEm-like cells and internal small dark stained cells resembling the embryonic portion (Figures 7A, 7B, S5B, and S5C). Consistently, immunostaining proximal cryosections of the same samples with the TROMA-I antibody showed positionally appropriate TROMA-I$^+$ cells surrounding TROMA-I$^-$ cells that we speculated to be Em-portion cells from their location and H&E-stain characteristics (Figure 7C), and other

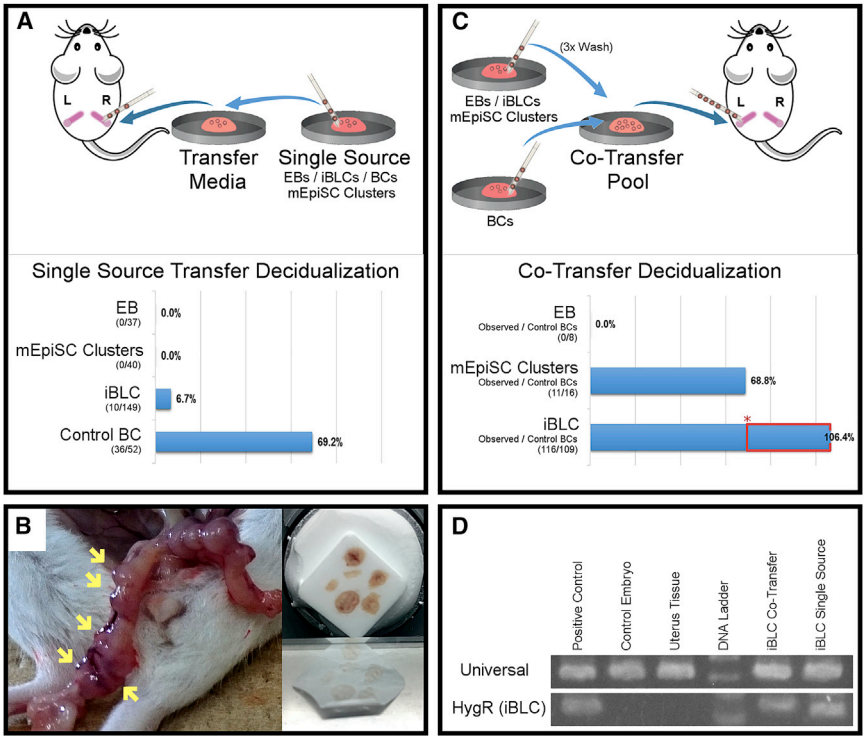


**Figure 6. iBLC Uterus Transfer Decidualization in Pseudopregnant Mice**

(A) Diagram of single-source uterus transfer experiment. Observed deciduae in uterus horns with respect to EBs, mEpiSC clusters, iBLCs, or control BCs single-source uterus transfers.

(B) Uterus horn of mouse with iBLC-implanted deciduae (left, yellow arrows), prepared for cryosection (right).

(C) Diagram of co-transfer experiment. Observed deciduae from EB co-transfer, mEpiSC Cluster co-transfer, and iBLC co-transfer. Asterisk denotes control BC decidualization rate (69.2%, A); red box indicates decidualization gained from iBLCs.

(D) Laser capture microdissection (LCM) genomic DNA PCR test for mouse genomic DNA universal and iBLC-specific hygromycin resistance. LCM sample regions from H&E slides are shown in Figure S5A.

In (A) and (C), embryo pipettes indicate when a new pipette was used.

TROMA-I$^+$ cells had further invaded the deciduae with TGC-like morphology (Figure 7C).

To further examine the development of iBLC-derived ExEm tissues in the deciduae, we immunostained for TPBPA and PL-I. Both were expressed in the cells lining and surrounding the embryonic chamber of iBLC-implanted deciduae, similarly to those in BC-derived tissues (Figure S5D) (Chen et al., 2016; Peng et al., 2015), and PL-I was also detected on control embryo ExEm visceral endoderm as reported previously (Figure S5D) (Chen et al., 2016). Several peripheral TPBPA$^+$ or PL-I$^+$ cells had larger, more brightly stained nuclei and were scattered far from the cavity. These cells could be polyploid-scattering TGCs, which were also suggested by the invading TROMA-I$^+$ cells (Figures 7C and S5D).

## DISCUSSION

We demonstrated here that PSCs can be reprogrammed to BC-like hemispheres with striking early embryonic implications, and we anticipate that cell conversions in such a context may be used to study early embryonic development *in vitro*. From this platform we modified the system to generate iBLCs with many similarities to BCs at morphological, developmental, molecular, and functional levels, although imperfect and perhaps less neatly regulated than the BC-like hemispheres (e.g., PrE regulation, Xi reactivation, pluripotency). Master transcription factors that establish, reprogram, and regulate cell fates in each lineage of BCs were expressed in iBLCs, and some (e.g., YAP, GATA3) were apparently correctly regulated. Notably, YAP is involved in both positional regulation and powerful gene regulation that can reprogram cell identity in numerous contexts (Panciera et al., 2016; Qin et al., 2016; Yu et al., 2016). iBLC system ICM-like masses had regulated nuclear-excluded YAP similar to natural BC ICM cells, which is a widely known characteristic difference from mouse ESCs in which YAP is nuclear enriched. iBLC implantation and growth *in utero* advances the prospect that important natural cues can be established in the system to later pass critically difficult natural barriers, even if dysregulation eventually caused embryonic resorption. The trend of the data suggests that developmental limitations in iBLCs may arise among heightened epigenetic plasticity that activates important genes weakly with poor regulation (e.g., OCT4, CDX2), perhaps causing latent or delayed lineage specification lacking distinct cell-identity resolution. The results point to diverging events for iBLCs and correcting the 2C-like establishment, and differentiation events could be the key to obtain fully functional iBLCs that develop further *in utero*. We provide comprehensive discussion of these data in Supplemental Discussion and a published preprint (Kime et al., 2018). Collectively, the current iBLC technology is a first step toward generating artificial isogenic BCs.

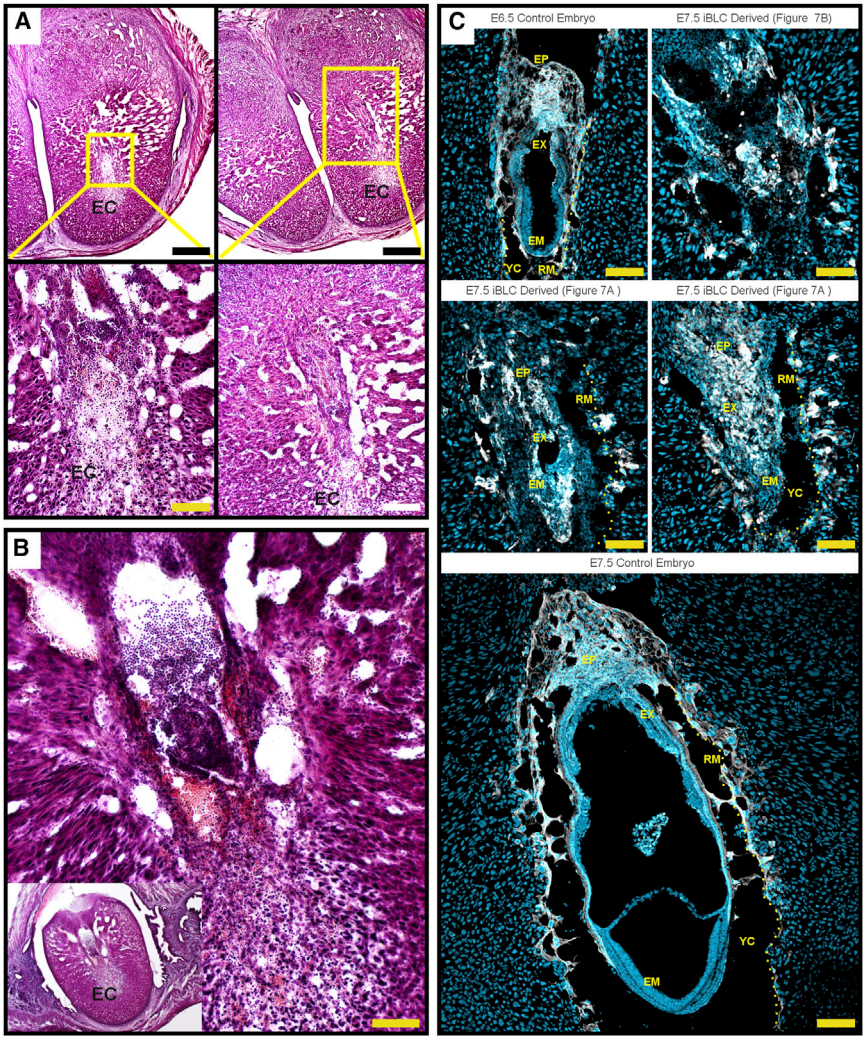


**Figure 7. iBLCs Implant and Partially Develop Before Resorption**

(A) H&E-stained proximal cryosections of deciduae from iBLC single-source transfer. Higher magnification is indicated and shows iBLC-derived tissue resembling large cell masses of resorbing tissues. EC, embryonic cavity. Scale bars, 500 μm (top panels), 100 μm (bottom left), and 200 μm (bottom right).

(B) H&E-stained decidua from iBLC single-source transfer showed high presence of immune cells resorbing a mass of cells with ExEm-like and Em-like stain and morphology. Scale bar, 100 μm.

(C) Cryosection stain for TROMA-I (white) and DNA (light blue). E6.5 and E7.5 control embryos show healthy size and structure. E7.5 iBLC-derived tissues from cryosections proximal to (A) and (B) are labeled. EP, ectoplacental cone; EX, extraembryonic portion; EM, embryonic portion; YC, yolk sac cavity; RM and dotted line, Reichert's membrane labeled on one side for clarity, as previously described on resorbing embryos (Cossée et al., 2000). Scale bars, 100 μm.

In previous work with mouse PSC-derived oogenesis, rare BC-like structures from >40-day long-term differentiation experiments, were briefly described (Hübner et al., 2003), although further characterization or competence *in utero* remains unknown. Two recently published systems for modeling early embryo development *in vitro* (Harrison et al., 2017; Rivron et al., 2018) expanded upon the reach of previously patented technology (Buhl et al., 2009). In such systems, ESCs and TSCs were precisely co-cultured to recapitulate embryo-like structures and highlight some of the increased developmental potential from lineage cooperation, as described from BC dissections decades prior (Gardner and Johnson, 1972). In great contrast, iBLCs self-organize and differentiate from 2C gene expressing iBLC-PCs, emerging only from primed PSCs in defined conditions.

Prdm14 is critical for germ-cell induction and fertility while important but dispensable in the embryonic PSC during development (Yamaji et al., 2008). On the contrary, Prdm14 may play a role in the earlier cleaving embryo where it is heterogeneously expressed, preceding discrete regulation to enrich the Em lineage during bifurcation (Burton et al., 2013). Given that the first phase of iBLC induction is akin to germ-cell induction from PSCs (Chen et al., 2012), we believe that the iBLC system failure from *Prdm14* KD arises from compromising the germ-cell program. The implicit germ-like *Prdm14* induction engaging iBLC-PC formation may be separated from the *Prdm14* expression in iBLCs that may depend on the iBLC quality. qRT-PCR assay detection is valuable and *Prdm14* detection in two out of six early iBLCs is a positive result, although not definitive.

The qRT-PCR assays used RNA extracted from single BCs and iBLCs. Unsurprisingly, iBLCs exhibited greater variations than BCs, yet one may appreciate that several important early embryo genes (*Cripto*, *Zfp42*, *Zscan4*, *Cdx2*,

*Sox17*, and *Gata3*) were activated in some or many individual iBLCs. When several iBLCs activated these genes, there was a commonality in the expression level that allows us to distinguish the system from a true BC, to understand it better, and to consider how it is further distanced from the starting mEpiSCs.

iBLCs may advance research in isogenic increased potential from PSCs, and we speculate that partial germ-lineage induction may be a causal link to the unique 2C-like transient expression seen in iBLC-PCs. Therein, early embryonic mimicry is autonomously installed in potentiated cells by a subsequent treatment with defined small molecules: iBLC-PCs can differentiate to iBLCs in the traditional embryo medium KSOM (data not shown).

Defined conditions that induce primed PSCs toward synchronous expression of 2C/*MERVL* reporter in clusters (iBLC-PC/loci) of cells that subsequently self-organize BC-like cysts are unique in the field of totipotency/2C-like cell research (Wu et al., 2017). *Zscan4* and *Tcstv3* evidence herein further implicates a 2C totipotency-related program in our system. Until now, 2C-like gene expression was only transiently expressed in individual rare cells among naive ESC cultures, and although bidirectional contribution of the traditional 2C-like *MERVL*$^{+}$ cells was shown in previous reports (Macfarlan et al., 2012), such cells remain unremarkably similar to ESCs in culture and require donor embryos to develop *in utero*: true isogenic totipotency from PSCs remains elusive. We anticipate that more precise control of cell reprogramming inputs may improve or stabilize the 2C-like program in iBLC-PCs to yield fully developed animals from PSCs alone and to maximize PSC reprogramming. Our methodology involves ~1 week of simplified defined media changes. Therefore, we envision that future iBLC technology may readily open avenues in several fields, such as embryology, 2C epigenetics, and implantation biology, in addition to its promise in early embryogenesis.

## EXPERIMENTAL PROCEDURES

### Experimental Model Details

Please refer to Supplemental Information for exact reagent/resource ordering information.

#### *Animal Use*

Mouse handling and experiments were carried out with humane methods in compliance with animal ethical standards approved by RIKEN Kobe Safety Center. Sterile-male bred pseudopregnant (PP) surrogate CD-1 (ICR) female mice were prepared at PP2.5 and then control BCs, iBLCs, mEpiSC clusters, or EBs were transferred to the uterus using standard embryo *in vitro* fertilization (IVF) pipetting techniques. CD-1 (ICR) BCs and R26-H2B-EGFP BCs were used for control BC experiments (Abe et al., 2011).

#### *Recombinant DNA Preparation*

We prepared RFP as dsRed, mCherry, and also a modified mCherry under the *EOS* reporter by adding a mouse ornithine decarboxylase destabilization domain (D2) (Li et al., 1998) and nuclear localization tags to the RFP (*EOS*::D2nRFP). D2 drastically reduces the half-life of the D2nRFP, providing timely live RFP responsiveness to mRNA level changes: the D2nRFP signal more closely represents OCT4/SOX2 heterodimer transcriptional activity. We also cloned RFP under the 2C *MERVL* reporter promoter. All reporter systems were cloned in piggybac vector systems with 5′ and 3′ insulators.

#### *mEpiSC Culture*

mEpiSC culture medium (MCM) consisted of NDiff227 supplemented with 20 ng/mL ActivinA, 12 ng/mL basic fibroblast growth factor, and 1:100 penicillin/streptomycin. Media and supplements were stored separately at −20°C in aliquots, freshly thawed at least every 4 days, and stored at 4°C. mEpiSC were cultured on plates previously coated for 1 h at room temperature with 1:100 fibronectin/PBS. Medium was changed daily, and cells were passaged as small clumps every 2–3 days at ~1:10–20, never exceeding 30% confluence. Cell colonies remained less than 300–400 μm wide and largely resembled homogeneous mEpiSC colonies with few single cells. Cell passage was carried out, in brief, with PBS wash, fresh Accutase for 55 s, PBS wash, 2 mL of MCM, scraped, triturated 6–8 times in a conical vial, then dispersed ~1:10–20 in MCM. If cells exhibited signs of differentiation, the culture was discarded and replaced by a freshly thawed stock.

### Method Details

#### *CTSFES Medium Preparation for Working Medium*

For preparation of ~1 L of CTSFES basal medium, 500 mL of DMEM:F12 + Glutamax, 500 mL of neurobasal medium, 10 mL of B27 supplement, 5 mL of N2 supplement, 5 mL of Glutamax supplement, and 670 μL of 7.5% BSA Frac V solution was filtered at 0.22 μm, aliquoted, and stored immediately at −20°C, thawed overnight at 4°C, and used for 1–8 days.

For CTSFES "working medium," after thawing for experimental use, 1:100 penicillin/streptomycin, 1:1000 2-ME, and 64 μg/mL ascorbic acid 2-phosphate were added.

#### *mEpiSC Preparation for Naive Conversion or iBLC Generation*

Target wells of 6W plate were coated with 1.5 mL of 1:100 fibronectin/PBS substrate for 1 h at room temperature. Stock cultures of near-passage mEpiSC colonies were sourced for passage into the conversion experiment as follows. Cells were washed with PBS, then treated with freshly thawed room-temperature Accutase for 1 min which was gently aspirated, and then cells were washed again with equal volume of PBS while tapping the plate gently to release single cells, and then PBS was gently aspirated again and replaced with 37°C prewarmed fresh Accutase and incubated at 37°C for 5–7 min until cells floated and dispersed freely. PBS/MCM (5× volume, 1:1) was added and the volume triturated 10–20 times in 15-mL conical vial. Cells were centrifuged at 200 × *g* for 3 min, then the mEpiSC pellet was resuspended in 1–2 mL of MCM, and live cells were counted. Cells were diluted in MCM to yield ~20,000 cells/1.5 mL for naive conversions or 30–50,000 cells/1.5 mL for iBLC generation, mixed evenly. Fibronectin/PBS coating was aspirated from target plates and 1.5 mL of diluted cells in MCM were added per well. Cells were

incubated at 37°C for 14–16 h before conversion medium was added; plates were often checked 2–3 h after plating to ensure cells plated as single evenly dispersed cells.

### *Naive Conversion Experiment*

For naive conversion experiment medium (NCM) (8 days of changes), working medium + (10 ng/mL bone morphogenetic protein 4 [BMP4], 1,000 units/mL ESGRO leukemia inhibitory factor [LIF], 1 μM (1-oleoyl-2-methyl-sn-glycero-3-phosphothionate ammonium salt [OMPT]) were prepared fresh at least every 4 days. 6W wells plated with ~20,000 mEpiSC cells/well were fed 2 mL of NCM daily starting ~14–16 h after cells were plated with the aforementioned preparation.

### *iBLC Generation Experiment*

For iBLC generation medium phase 1, day 0–3 medium (4 changes), working medium + (10 ng/mL BMP4, 1 μM SB43152) was prepared fresh on day 0, and SB431542 was increased to 3 μM for days 1–3.

For iBLC generation medium phase 2, day 4–6 medium (3 changes), working medium + (5 ng/mL BMP4, 500–1,000 units/mL ESGRO LIF, 0.5–1 μM OMPT) were prepared fresh on day 4.

6W wells plated with 30–50,000 mEpiSC cells/well were fed 2 mL of phase 1 medium daily at a similar time, starting 14–16 h after cells were plated using the aforementioned preparation method. From day 4, 2 mL of phase 2 medium was changed daily. On day 6 and day 7, iBLC-PCs and some emerging iBLCs were collected with ART P1000G wide-bore pipette tips. The iBLC generation plate was leaned at a 45° angle, and the upper 1 mL (primary) was harvested to one well of a 24-well ultralow attachment (ULA) plate; the lower 1 mL (secondary) was drawn up and cascaded over the plate once and then harvested to a separate well of a 24-well ULA plate. Two milliliters of phase 2 medium was replaced on the plate if the culture was observed or used later. Some iBLC experiments included 0.2 μM sodium pyruvate. In a few experiments, SB431542 was varied between 1 and 10 μM, and phase 1 and phase 2 media were mixed 1:1 on days 3, 4, or 5.

Primary and secondary harvests from one 6W well of iBLC generation were considered together, although secondary harvests contained more iBLC-PCs, iBLCs, and cell debris. Early on day 7, primary and secondary harvests were observed for brief periods, and the emergence of morula-like structures and early blastocyst-like structures from iBLC-PCs was noted on the 24W ULA plate lid. Working medium or phase 2 medium was placed in a Hydrocell 3.5-cm plate and incubated for ~1 h at 37°C. iBLCs were judged by morphology for blastocyst-like characteristics and isolated by embryo transfer pipette to the Hydrocell 3.5-cm plate and incubated for 1–3 h at 37°C. The Hydrocell 3.5-cm plate of near-completely purified iBLCs was then sourced for analysis or IVF transfer into PP2.5 sterile-male bred pseudopregnant mice. When iBLCs were transferred to pseudopregnant mice, they were washed three times by transfer into separate drops of standard embryo transfer medium. In such transfers, unique glass pipettes were used between each step to ensure sample-handling accuracy.

## SUPPLEMENTAL INFORMATION

Supplemental Information can be found online at https://doi.org/10.1016/j.stemcr.2019.07.011.

## AUTHOR CONTRIBUTIONS

Conceptualization, C.K.; Methodology, C.K. and K.T.; Cryosections, C.K. and E.K.; Validation, S.O.; Formal Analysis, C.K. and K.T.; Investigation, C.K., K.T., and H.K.; Resources, C.K., K.T., S.Y., and M.T.; Writing – Original Draft, C.K. and K.T.; Writing – Revision & Editing, C.K. and K.T.; Visualization, C.K.; Supervision, C.K. and K.T.; Project Administration, C.K.; Funding Acquisition, C.K., K.T., S.Y., M.A., and M.T.

## CONFLICTS OF INTEREST

C.K. and K.T. have patents related to this technology and extended works. S.Y. is a scientific advisor of iPS Academia Japan without salary.

## ACKNOWLEDGMENTS

We honor the help of Dr. Hitoshi Niwa for critical input and for providing the rabbit anti-mouse CDX2 antibody. We are grateful to Drs. Siqin Bao and Azim Surani for their female XGFP mEpiSC. We also thank Drs. Robert Blelloch and Paul Tesar for providing their mEpiSC for research. MERVL 2C and EOS-S(4+) reporter DNA was provided by Addgene (http://www.addgene.org) under MTA and subcloned into our systems. TROMA-I (Krt8) monoclonal antibody developed by Institut Pasteur was obtained from the Developmental Studies Hybridoma Bank (DSHB), created by the NICHD of the NIH and maintained at the Department of Biology, University of Iowa. We greatly thank the Yamanaka and Takahashi labs for the support and research environment that made this work possible. We also thank Michael Kime for producing the graphical abstract artwork in Figure 1. This work was supported by funding from RIKEN, Kyoto University, and the Gladstone Institutes; L.K. Whittier Foundation and the Roddenberry Foundation; National Heart, Lung, and Blood Institute/NIH grants U01-HL100406 and U01-HL098179; and from the California Institute for Regenerative Medicine (CIRM). The Gladstone Institutes received support from a National Center for Research Resources Grant RR18928-01. C.K. was supported in part by the RIKEN SPDR program. K.T. was supported in part by JSPS KAKENHI grant 17K07246 and the Suzuki Memorial Foundation. M.A was supported in part by an OMC Internal Research Grant.

Received: January 4, 2019
Revised: July 9, 2019
Accepted: July 15, 2019
Published: August 8, 2019

## REFERENCES

Abe, T., Kiyonari, H., Shioi, G., Inoue, K.-I., Nakao, K., Aizawa, S., and Fujimori, T. (2011). Establishment of conditional reporter mouse lines at ROSA26 locus for live cell imaging. Genesis *49*, 579–590.

Akiyama, T., Xin, L., Oda, M., Sharov, A.A., Amano, M., Piao, Y., Cadet, J.S., Dudekula, D.B., Qian, Y., Wang, W., et al. (2015). Transient bursts of Zscan4 expression are accompanied by the rapid derepression of heterochromatin in mouse embryonic stem cells. DNA Res. *22*, 307–318.

Bao, S., Tang, F., Li, X., Hayashi, K., Gillich, A., Lao, K., and Surani, M.A. (2009). Epigenetic reversion of post-implantation epiblast to pluripotent embryonic stem cells. Nature *461*, 1292–1295.

Bedzhov, I., Graham, S.J.L., Leung, C.Y., and Zernicka-Goetz, M. (2014). Developmental plasticity, cell fate specification and morphogenesis in the early mouse embryo. Philos. Trans. R. Soc. Lond. B Biol. Sci. *369*, 20130538.

Benchetrit, H., Jaber, M., Zayat, V., Sebban, S., Pushett, A., Makedonski, K., Zakheim, Z., Radwan, A., Maoz, N., Lasry, R., et al. (2019). Direct induction of the three pre-implantation blastocyst cell types from fibroblasts. Cell Stem Cell *24*, 983–994.

Buhl, S., Egert, A., Schorle, H., and Woynecki, T. (2009). Induced blastocyst-like structures, methods of production and uses of the same. European patent EP2088191A1, filed February 8, 2008.

Bulut-Karslioglu, A., Biechele, S., Jin, H., Macrae, T.A., Hejna, M., Gertsenstein, M., Song, J.S., and Ramalho-Santos, M. (2016). Inhibition of mTOR induces a paused pluripotent state. Nature *540*, 119–123.

Burton, A., Muller, J., Tu, S., Padilla-Longoria, P., Guccione, E., and Torres-Padilla, M.-E. (2013). Single-cell profiling of epigenetic modifiers identifies PRDM14 as an inducer of cell fate in the mammalian embryo. Cell Rep. *5*, 687–701.

Cha, J., Sun, X., and Dey, S.K. (2012). Mechanisms of implantation: strategies for successful pregnancy. Nat. Med. *18*, 1754–1767.

Chen, W., Jia, W., Wang, K., Zhou, Q., Leng, Y., Duan, T., and Kang, J. (2012). Retinoic acid regulates germ cell differentiation in mouse embryonic stem cells through a Smad-dependent pathway. Biochem. Biophys. Res. Commun. *418*, 571–577.

Chen, C.-Y., Chan, C.-H., Chen, C.-M., Tsai, Y.-S., Tsai, T.-Y., Wu Lee, Y.-H., and You, L.-R. (2016). Targeted inactivation of murine Ddx3x: essential roles of Ddx3x in placentation and embryogenesis. Hum. Mol. Genet. *25*, 2905–2922.

Cossée, M., Puccio, H., Gansmuller, A., Koutnikova, H., Dierich, A., LeMeur, M., Fischbeck, K., Dollé, P., and Kœnig, M. (2000). Inactivation of the Friedreich ataxia mouse gene leads to early embryonic lethality without iron accumulation. Hum. Mol. Genet. *9*, 1219–1226.

Czechanski, A., Byers, C., Greenstein, I., Schrode, N., Donahue, L.R., Hadjantonakis, A.-K., and Reinholdt, L.G. (2014). Derivation and characterization of mouse embryonic stem cells from permissive and nonpermissive strains. Nat. Protoc. *9*, 559–574.

Falco, G., Lee, S.-L., Stanghellini, I., Bassey, U.C., Hamatani, T., and Ko, M.S.H. (2007). Zscan4: a novel gene expressed exclusively in late 2-cell embryos and embryonic stem cells. Dev. Biol. *307*, 539–550.

Flores, L.E., Hildebrandt, T.B., Kühl, A.A., and Drews, B. (2014). Early detection and staging of spontaneous embryo resorption by ultrasound biomicroscopy in murine pregnancy. Reprod. Biol. Endocrinol. *12*, 38.

Gardner, R.L., and Johnson, M.H. (1972). An investigation of inner cell mass and trophoblast tissues following their isolation from the mouse blastocyst. Development *28*, 279–312.

Guo, G., Huss, M., Tong, G.Q., Wang, C., Li Sun, L., Clarke, N.D., and Robson, P. (2010). Resolution of cell fate decisions revealed by single-cell gene expression analysis from zygote to blastocyst. Dev. Cell *18*, 675–685.

Hackett, J.A., Kobayashi, T., Dietmann, S., and Surani, M.A. (2017). Activation of lineage regulators and transposable elements across a pluripotent spectrum. Stem Cell Reports *8*, 1645–1658.

Harrison, S.E., Sozen, B., Christodoulou, N., Kyprianou, C., and Zernicka-Goetz, M. (2017). Assembly of embryonic and extraembryonic stem cells to mimic embryogenesis in vitro. Science *356*, eaal1810.

Hiller, M., Liu, C., Blumenthal, P.D., Gearhart, J.D., and Kerr, C.L. (2010). Bone morphogenetic protein 4 mediates human embryonic germ cell derivation. Stem Cells Dev. *20*, 351–361.

Hirate, Y., Hirahara, S., Inoue, K., Kiyonari, H., Niwa, H., and Sasaki, H. (2015). Par-aPKC-dependent and -independent mechanisms cooperatively control cell polarity, Hippo signaling, and cell positioning in 16-cell stage mouse embryos. Dev. Growth Differ. *57*, 544–556.

Home, P., Ray, S., Dutta, D., Bronshteyn, I., Larson, M., and Paul, S. (2009). GATA3 is selectively expressed in the trophectoderm of peri-implantation embryo and directly regulates Cdx2 gene expression. J. Biol. Chem. *284*, 28729–28737.

Hotta, A., Cheung, A.Y.L., Farra, N., Vijayaragavan, K., Séguin, C.A., Draper, J.S., Pasceri, P., Maksakova, I.A., Mager, D.L., Rossant, J., et al. (2009). Isolation of human iPS cells using EOS lentiviral vectors to select for pluripotency. Nat. Methods *6*, 370–376.

Hübner, K., Fuhrmann, G., Christenson, L.K., Kehler, J., Reinbold, R., Fuente, R.D.L., Wood, J., Strauss, J.F., Boiani, M., and Schöler, H.R. (2003). Derivation of oocytes from mouse embryonic stem cells. Science *300*, 1251–1256.

Kime, C., Sakaki-Yumoto, M., Goodrich, L., Hayashi, Y., Sami, S., Derynck, R., Asahi, M., Panning, B., Yamanaka, S., and Tomoda, K. (2016). Autotaxin-mediated lipid signaling intersects with LIF and BMP signaling to promote the naive pluripotency transcription factor program. Proc. Natl. Acad. Sci. U S A *113*, 12478–12483.

Kime, C., Kiyonari, H., Ohtsuka, S., Kohbayashi, E., Asahi, M., Yamanaka, S., Takahashi, M., and Tomoda, K. (2018). Implantation-competent blastocyst-like structures from mouse pluripotent stem cells. BioRxiv https://doi.org/10.1101/309542.

Latos, P.A., and Hemberger, M. (2016). From the stem of the placental tree: trophoblast stem cells and their progeny. Development *143*, 3650–3660.

Li, X., Zhao, X., Fang, Y., Jiang, X., Duong, T., Fan, C., Huang, C.-C., and Kain, S.R. (1998). Generation of destabilized green fluorescent protein as a transcription reporter. J. Biol. Chem. *273*, 34970–34975.

Luna-Zurita, L., and Bruneau, B.G. (2013). Chromatin modulators as facilitating factors in cellular reprogramming. Curr. Opin. Genet. Dev. *23*, 556–561.

Macfarlan, T.S., Gifford, W.D., Agarwal, S., Driscoll, S., Lettieri, K., Wang, J., Andrews, S.E., Franco, L., Rosenfeld, M.G., Ren, B., et al. (2011). Endogenous retroviruses and neighboring genes are coordinately repressed by LSD1/KDM1A. Genes Dev. *25*, 594–607.

Macfarlan, T.S., Gifford, W.D., Driscoll, S., Lettieri, K., Rowe, H.M., Bonanomi, D., Firth, A., Singer, O., Trono, D., and Pfaff, S.L. (2012).

Embryonic stem cell potency fluctuates with endogenous retrovirus activity. Nature *487*, 57–63.

Mochida, K., Hasegawa, A., Otaka, N., Hama, D., Furuya, T., Yamaguchi, M., Ichikawa, E., Ijuin, M., Taguma, K., Hashimoto, M., et al. (2014). Devising assisted reproductive technologies for wild-derived strains of mice: 37 strains from five subspecies of Mus musculus. PLoS One *9*, e114305.

Monk, M., and Harper, M.I. (1979). Sequential X chromosome inactivation coupled with cellular differentiation in early mouse embryos. Nature *281*, 311–313.

Morgani, S.M., and Brickman, J.M. (2015). LIF supports primitive endoderm expansion during pre-implantation development. Development *142*, 3488–3499.

Nakaki, F., and Saitou, M. (2014). PRDM14: a unique regulator for pluripotency and epigenetic reprogramming. Trends Biochem. Sci. *39*, 289–298.

Nishioka, N., Inoue, K., Adachi, K., Kiyonari, H., Ota, M., Ralston, A., Yabuta, N., Hirahara, S., Stephenson, R.O., Ogonuki, N., et al. (2009). The hippo signaling pathway components lats and yap pattern tead4 activity to distinguish mouse trophectoderm from inner cell mass. Dev. Cell *16*, 398–410.

Norwitz, E.R., Schust, D.J., and Fisher, S.J. (2001). Implantation and the survival of early pregnancy. N. Engl. J. Med. *345*, 1400–1408.

Ohinata, Y., and Tsukiyama, T. (2014). Establishment of trophoblast stem cells under defined culture conditions in mice. PLoS One *9*, e107308.

Ohtsuka, S., Nishikawa-Torikai, S., and Niwa, H. (2012). E-Cadherin promotes incorporation of mouse epiblast stem cells into normal development. PLoS One *7*, e45220.

Okamoto, I., Otte, A.P., Allis, C.D., Reinberg, D., and Heard, E. (2004). Epigenetic dynamics of imprinted X inactivation during early mouse development. Science *303*, 644–649.

Panciera, T., Azzolin, L., Fujimura, A., Di Biagio, D., Frasson, C., Bresolin, S., Soligo, S., Basso, G., Bicciato, S., Rosato, A., et al. (2016). Induction of expandable tissue-specific stem/progenitor cells through transient expression of YAP/TAZ. Cell Stem Cell *19*, 725–737.

Parchem, R.J., Ye, J., Judson, R.L., LaRussa, M.F., Krishnakumar, R., Blelloch, A., Oldham, M.C., and Blelloch, R. (2014). Two miRNA clusters reveal alternative paths in late-stage reprogramming. Cell Stem Cell *14*, 617–631.

Payer, B., Lee, J.T., and Namekawa, S.H. (2011). X-inactivation and X-reactivation: epigenetic hallmarks of mammalian reproduction and pluripotent stem cells. Hum. Genet. *130*, 265–280.

Peng, J., Fullerton, P.T., Monsivais, D., Clementi, C., Su, G.H., and Matzuk, M.M. (2015). Uterine activin-like kinase 4 regulates trophoblast development during mouse placentation. Mol. Endocrinol. *29*, 1684–1693.

Plusa, B., Piliszek, A., Frankenberg, S., Artus, J., and Hadjantonakis, A.-K. (2008). Distinct sequential cell behaviours direct primitive endoderm formation in the mouse blastocyst. Development *135*, 3081–3091.

Qin, H., Hejna, M., Liu, Y., Percharde, M., Wossidlo, M., Blouin, L., Durruthy-Durruthy, J., Wong, P., Qi, Z., Yu, J., et al. (2016). YAP induces human naive pluripotency. Cell Rep. *14*, 2301–2312.

Ralston, A., and Rossant, J. (2008). Cdx2 acts downstream of cell polarization to cell-autonomously promote trophectoderm fate in the early mouse embryo. Dev. Biol. *313*, 614–629.

Rings, E.H.H.M., Boudreau, F., Taylor, J.K., Moffett, J., Suh, E.R., and Traber, P.G. (2001). Phosphorylation of the serine 60 residue within the Cdx2 activation domain mediates its transactivation capacity. Gastroenterology *121*, 1437–1450.

Rivron, N.C., Frias-Aldeguer, J., Vrij, E.J., Boisset, J.-C., Korving, J., Vivié, J., Truckenmüller, R.K., van Oudenaarden, A., van Blitterswijk, C.A., and Geijsen, N. (2018). Blastocyst-like structures generated solely from stem cells. Nature *557*, 106–111.

Saiz, N., and Plusa, B. (2013). Early cell fate decisions in the mouse embryo. Reproduction *145*, R65–R80.

Seydoux, G., and Braun, R.E. (2006). Pathway to totipotency: lessons from germ cells. Cell *127*, 891–904.

Stephenson, R.O., Yamanaka, Y., and Rossant, J. (2010). Disorganized epithelial polarity and excess trophectoderm cell fate in preimplantation embryos lacking E-cadherin. Development *137*, 3383–3391.

Steward, F.C., Mapes, M.O., and Mears, K. (1958). Growth and organized development of cultured cells. II. Organization in cultures grown from freely suspended cells. Am. J. Bot. *45*, 705–708.

Tesar, P.J., Chenoweth, J.G., Brook, F.A., Davies, T.J., Evans, E.P., Mack, D.L., Gardner, R.L., and McKay, R.D. (2007). New cell lines from mouse epiblast share defining features with human embryonic stem cells. Nature *448*, 196–199.

Tomioka, M., Nishimoto, M., Miyagi, S., Katayanagi, T., Fukui, N., Niwa, H., Muramatsu, M., and Okuda, A. (2002). Identification of Sox-2 regulatory region which is under the control of Oct-3/4–Sox-2 complex. Nucleic Acids Res. *30*, 3202–3213.

Wu, J., Huang, B., Chen, H., Yin, Q., Liu, Y., Xiang, Y., Zhang, B., Liu, B., Wang, Q., Xia, W., et al. (2016). The landscape of accessible chromatin in mammalian preimplantation embryos. Nature *534*, 652–657.

Wu, G., Lei, L., and Schöler, H.R. (2017). Totipotency in the mouse. J. Mol. Med. *95*, 1–8.

Yamaji, M., Seki, Y., Kurimoto, K., Yabuta, Y., Yuasa, M., Shigeta, M., Yamanaka, K., Ohinata, Y., and Saitou, M. (2008). Critical function of Prdm14 for the establishment of the germ cell lineage in mice. Nat. Genet. *40*, 1016–1022.

Yang, S., Yuan, Q., Niu, M., Hou, J., Zhu, Z., Sun, M., Li, Z., and He, Z. (2017). BMP4 promotes mouse iPS cell differentiation to male germ cells via Smad1/5, Gata4, Id1 and Id2. Reproduction *153*, 211–220.

Yu, C., Ji, S.-Y., Dang, Y.-J., Sha, Q.-Q., Yuan, Y.-F., Zhou, J.-J., Yan, L.-Y., Qiao, J., Tang, F., and Fan, H.-Y. (2016). Oocyte-expressed yes-associated protein is a key activator of the early zygotic genome in mouse. Cell Res. *26*, 275–287.

**Stem Cell Reports, Volume *13***

## Supplemental Information

# Induced 2C Expression and Implantation-Competent Blastocyst-like Cysts from Primed Pluripotent Stem Cells

**Cody Kime, Hiroshi Kiyonari, Satoshi Ohtsuka, Eiko Kohbayashi, Michio Asahi, Shinya Yamanaka, Masayo Takahashi, and Kiichiro Tomoda**

# SUPPLEMENTAL INFORMATION

## INVENTORY

# SUPPLEMENTAL FIGURES

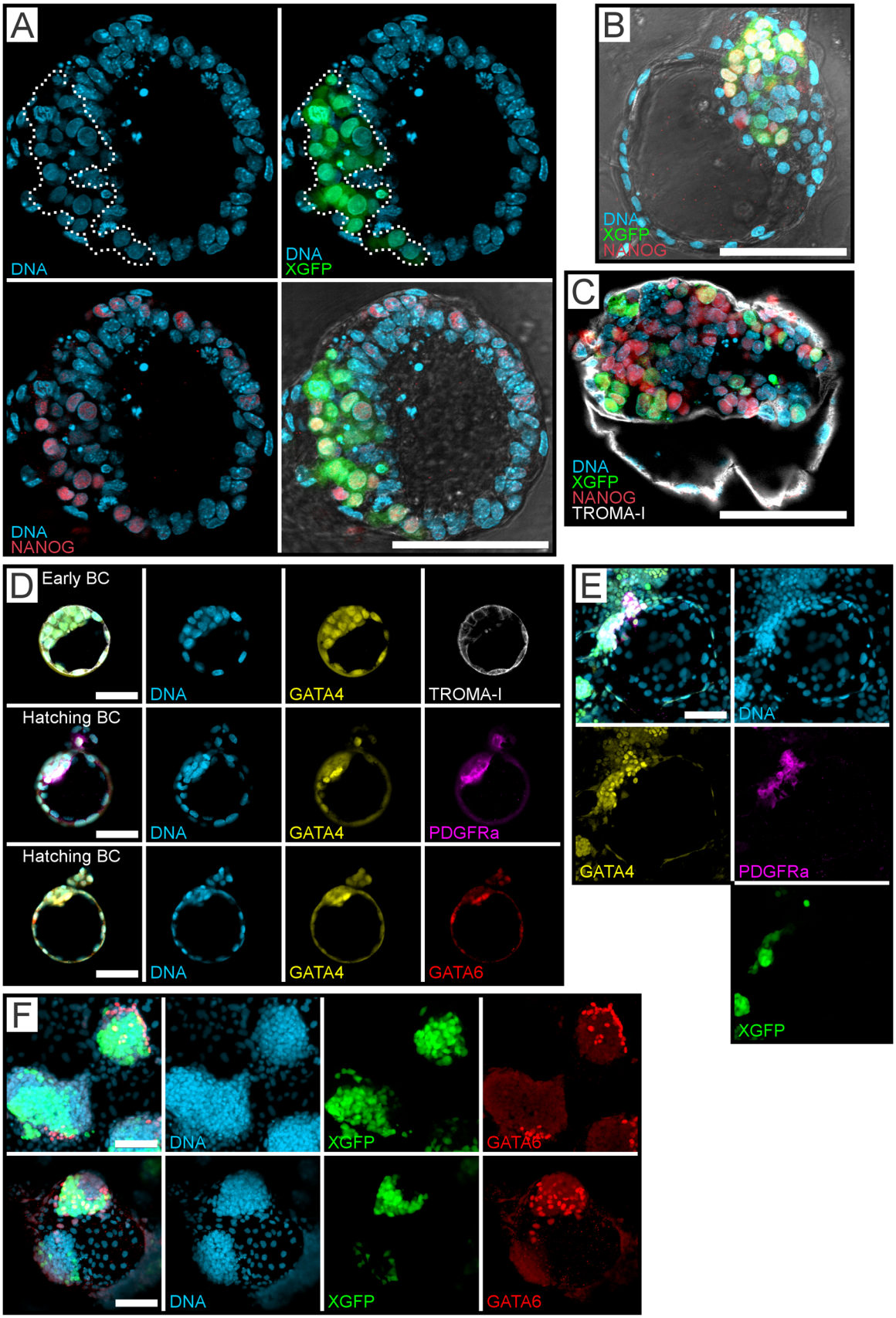

**Figure S1. Cell Conversion Induces Blastocyst-Like Hemispheres**
**Related to Figure 1, Figure 4, and Figure S3**

**A,B,C)** DNA (light blue), XGFP (green), and NANOG (red). Scale bars, 100 µm.

**A)** Oversized BC-like hemisphere with NANOG+XGFP+ inner cells, NANOG+XGFP-spheroid cells, and NANOG-XGFP- outer flattened TE-like cells. XGFP+ cells exclusively indicate euchromatin characteristics (white dotted outline) and XGFP- cells have bright DNA stain puncta indicating condensed DNA heterochromatin.

**B)** Late BC-like hemisphere cyst with NANOG+ cells restricted to XGFP+ cells surrounded by NANOG-XGFP- TE-like cells.

**C)** TE lineage marker positive cells (white; TROMA-I) surrounding the fluid filled hemisphere with large NANOG+XGFP+ polar mass.

**D)** Early BC (top) and late hatching BC (mid/bottom) stained for DNA (light blue), GATA4 (yellow), TROMA-I (white), PDGFRa (magenta), and GATA6 (red). Scale bars, 50 µm.

**E)** BC-like hemisphere XGFP (green) stained for DNA (light blue), GATA4 (yellow), TROMA-I (white), PDGFRa (magenta), and GATA6 (red). Scale bars, 100 µm.

**F)** Naive PSC-like colonies (top) and BC-like hemisphere (bottom) with XGFP (green), stained for DNA (light blue) and GATA6 (red). Scale bars, 100 µm.

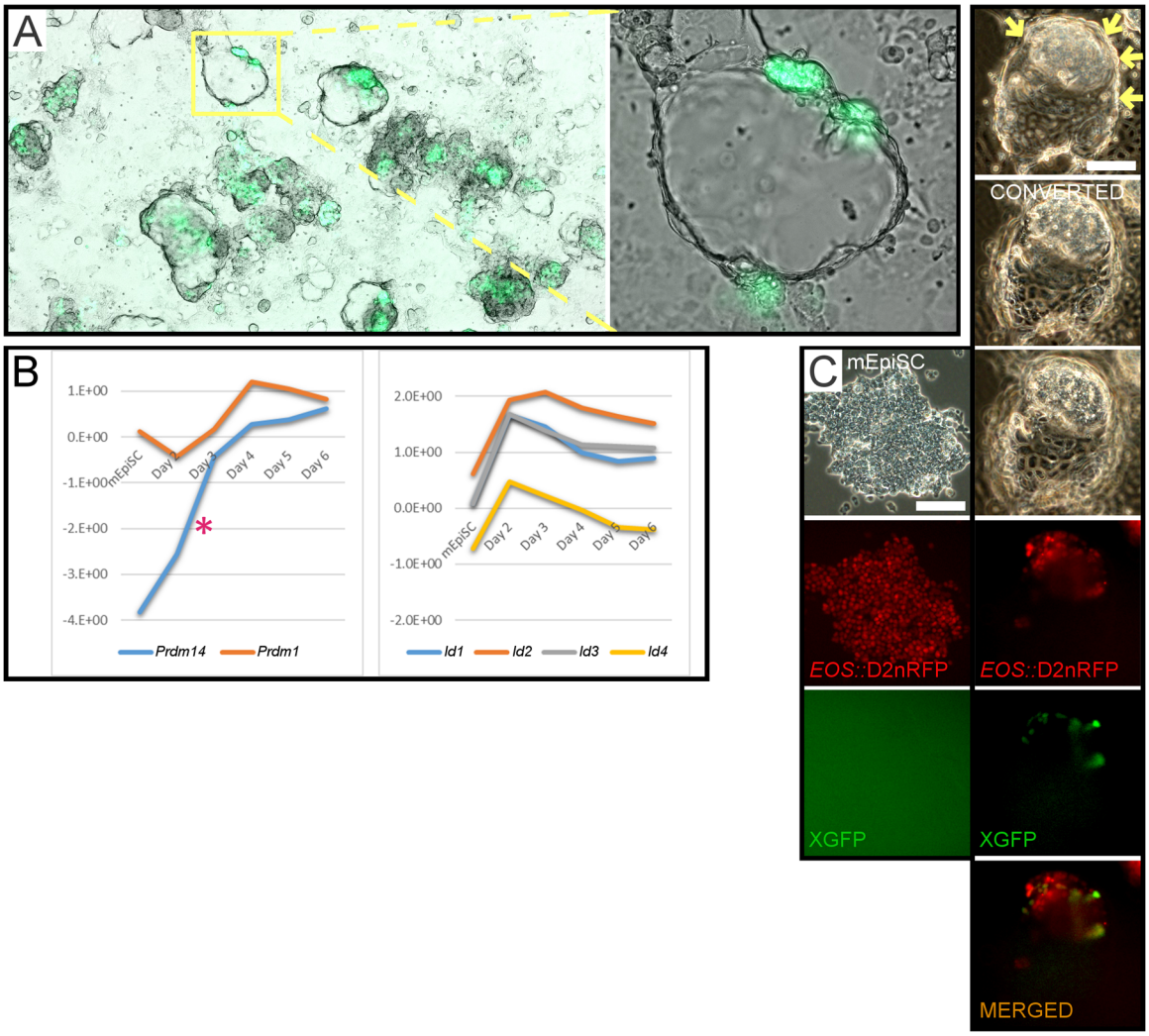


**Figure S2. Cell Conversion Induces Blastocyst-Like Hemispheres and Prdm and Id Gene mRNAs. Related to Figure S1 and Figure 4**

**A)** X chromosome reactivation indicated by XGFP+ cells as polar masses among numerous fluid filled BC-like hemispheres in naive conversion experiments.

**B)** qRT-PCR of naive conversion time course cDNA samples shows strong induction of *Id* genes in two days (right). *Prdm14* is induced from near undetectable signal in mEpiSC and *Prdm1 (Blimp1)* shows ~10-fold increase after 4 days (left). **Prdm14 time-course was previously reported* (Kime et al., 2016).

**C)** Naive conversion BC-like hemisphere with *EOS::*D2nRFP+ expression restricted to the putative ICM surrounded by TE-like cells (yellow arrows), across three Z-positions. Scale bar, 100 µm. *Note: mEpiSC green channel was drastically over-contrasted to show the absence of XGFP expression.*

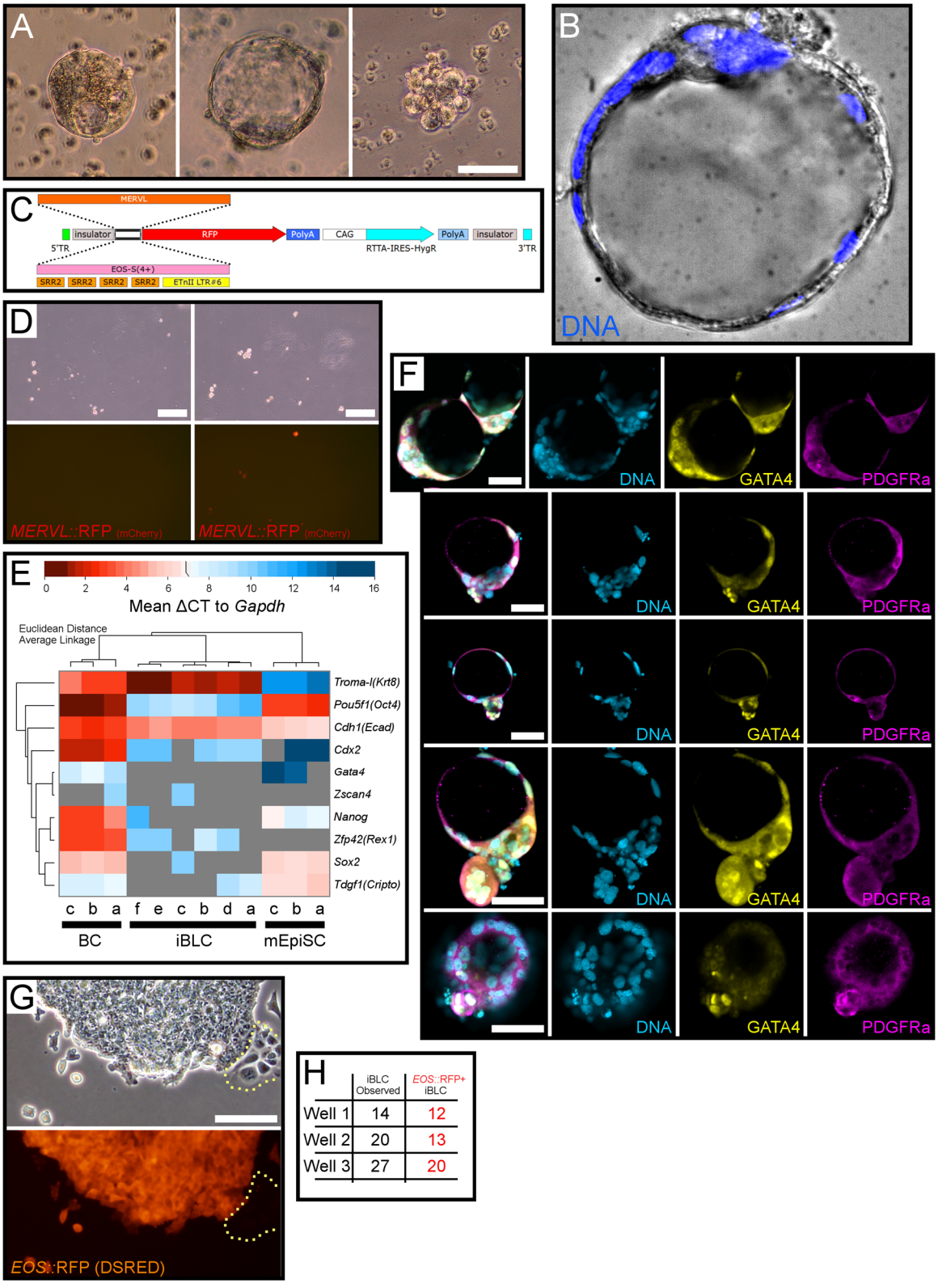


**Figure S3. iBLC System Extended Characterization, Reporter Constructs, and PrE-like Cell Localization**
**Related to Figures 1,2,4, and 5**

**A)** Early embryo-like structures are released to suspension. Scale bar, 50 µm.
**B)** Late iBLC stained for DNA (blue).
**C)** Schematic of piggyback reporter systems in this study: *MERVL* or *EOS-S(4+)* synthetic promoters followed by RFP. *RFP used are DSRED, mCherry, or D2nRFP (see Methods).*
**D)** *MERVL::*RFP reporter mEpiSC derived possible iBLC-PC collected on Day 6 and pooled based on RFP- or RFP+ expression. Scale bars, 500 µm.
**E)** qRT-PCR of individual early BC, early iBLC, and mEpiSC colony cDNA samples, with Euclidean distance and clustering by average linkage, represented as a heat map of ΔCT to *Gapdh*. *Note: We encountered low qRT-PCR Gata4 assay sensitivity which was detected far lower in control BCs than other reports (Guo et al., 2010) and was not detected in iBLCs despite significant immunocytochemical detection shown in Figure 4D, Figure S3F, and validated in Figure S1D.*
**F)** Numerous late iBLC stained for DNA (light blue), GATA4 (yellow), and PDGFRa (magenta). Scale bars, 50 µm. *Bottom image is taken from a rotated position with ICM-like mass toward the microscope lens.*
**G)** *EOS::*RFP+ mEpiSC and *EOS::*RFP- differentiating cells. *Differentiating cells are outlined with yellow dotted line.* Scale bar, 100 µm.
**H)** 6W wells of iBLC generation were harvested to ULA plates on Day 6, and counted on Day 7 as total and as *EOS::*RFP+.

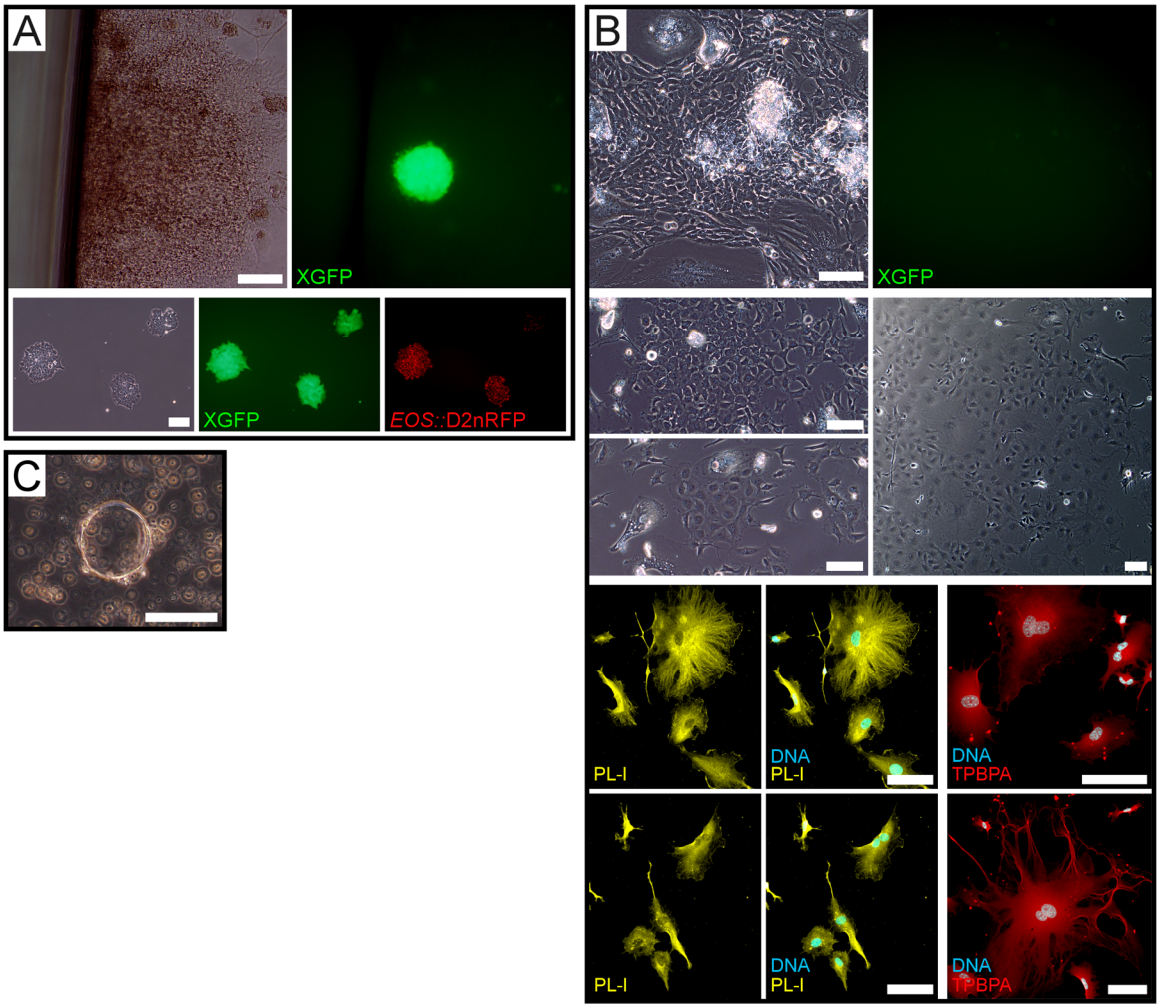


**Figure S4. iBLC System Outgrowth and Extended Characterization**
**Related to Figure 5**

**A)** *EOS::*D2nRFP mEpiSC induced iBLC and iBLC-PC were plated on feeders in ESC derivation conditions. Outgrowths reactivated the XGFP reporter (top) and stabilized similar to ESC after several passages and maintained XGFP and *EOS::*D2nRFP expression (bottom). Scale bars, 100 µm.

**B)** *EOS::*D2nRFP mEpiSC induced iBLC and iBLC-PC were plated on feeders in TE cell-culture conditions. Outgrowths mostly did not activate the XGFP reporter (top) and expanded for two passages into TE-like and TGC-like binuclear cells (middle). Cells were passaged to slides and stained for post-implantation ExEm cell markers PL-I (yellow), TPBPA (red), and DNA (light blue). Scale bars, 100 µm.

**C)** iBLC induced from another published mEpiSC line (Tesar et al., 2007). Scale bar, 100 µm.

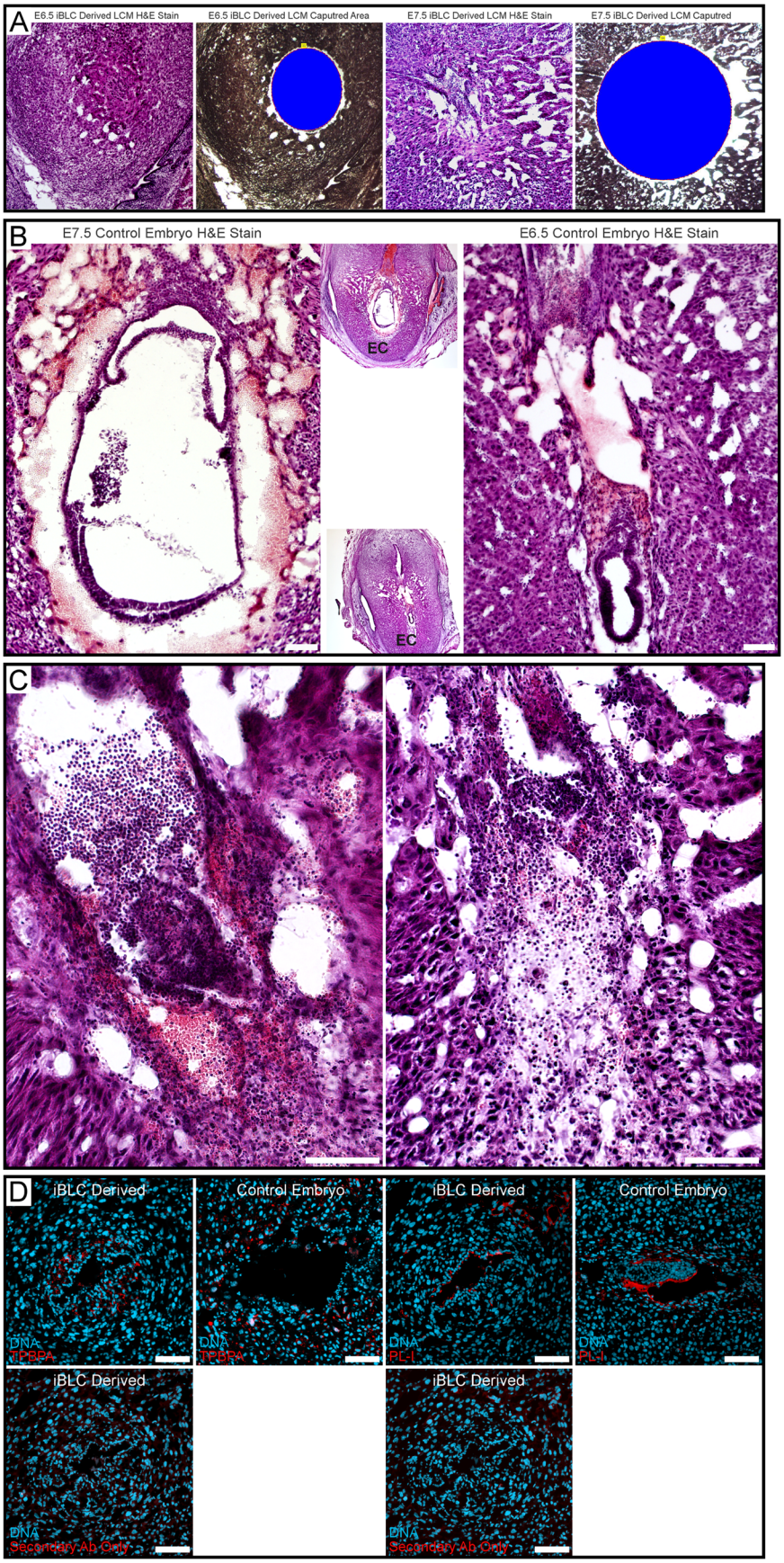

**Figure S5. Implanted Resorbing iBLC Derived Tissue and Healthy Control Embryos**
**Related to Figure 6 and Figure 7**
**A)** H&E stain and LCM sampled areas (blue fill) of proximal sections from implanted E6.5 iBLC co-transfer tissues (left) and E7.5 iBLC single source transfer (right). *LCM samples were used for genomic DNA PCR in Figure 6D.*
**B)** H&E stain for E7.5 and E6.5 control embryos for reference (large) with lower magnification images of the complete decidua section in uterine tissue (inset). *EC, embryonic cavity.* Scale bars, 100 µm.
**C)** Larger images of H&E stain for E7.5 iBLC single source transfer implanted tissue cryosections. Deciduae had many blood sinuses and ExEm-like cells at the periphery of resorbing tissue. Maternal immune cells were highly present throughout the area and accumulated from the blood sinuses. Loosely arranged ExEm-like cells appeared to retract within a degrading embryonic cavity and surrounding small darker stained cells resembling the Em cells seen in healthy control embryos (Figure S5B). Scale bars, 100 µm.
**D)** Embryonic cavity cryosection stain of iBLC derived and control embryo cells for post-implantation ExEm lineage markers TPBPA and PL-I (red) with DNA (light blue). Proximal sections were stained without primary antibodies and shown as negative controls (bottom). Scale bars, 100 µm.

# SUPPLEMENTAL VIDEO

**Video S1. Blastocyst-Like Hemisphere Imaged from Z-stack**
**Related to Figure S1**
A late BC-like hemisphere imaged across the z-dimension, visualized as a composite 3D model and animated for viewing from several angles. XGFP+NANOG+ cells are restricted to a polar mass of the fluid filled dome surrounded by large flat cells with large flat nuclei. XGFP (green), NANOG (red), and DNA (blue).

# SUPPLEMENTAL TABLES

| iBLC Observed Date * | Relative Yield ** |
|---|---|
| 10/25/2014 | + |
| 11/25/2014 | + |
| 12/27/2014 | + |
| 7/14/2015 | + |
| 8/4/2015 | + |
| 10/21/2015 | + |
| 10/28/2015 | + |
| 2/26/2016 | + |
| 3/17/2016 | ++ |
| 3/31/2016 | ++ |
| 5/12/2016 | ++ |
| 6/13/2016 | ++ |
| 9/15/2016 | ++ |
| 10/27/2016 | ++ |
| 11/17/2016 | +++ |
| 1/8/2017 | +++ |
| 2/8/2017 | ++ |
| 4/25/2017 | ++ |
| 5/11/2017 | ++ |
| 6/21/2017 | ++ |
| 12/8/2017 | ++ |
| 12/26/2017 | +++ |
| 1/7/2018 | ++ |
| 8/17/2018 | + |
| 11/21/2019 | ++ |
| 11/22/2019 | + |
| 1/17/2019 | ++ |
| 4/23/2019 | + |
| 5/1/2019 | +++ |

*May include 1-2 days after because iBLC-PC can be harvested each day for approximately 2 days and become iBLCs ~12-48 hours later in suspension.
**Differences in relative yield reflect experiment optimization changes.
Experiments with + yield usually had ~2-5 iBLCs from one 6W well.
Experiments with ++ yield usually had ~10-30 iBLCs from one 6W well and were preferable.
Experiments with +++ yield were so abundant that iBLCs readily aggregated and complicated purification.

**Table S1. iBLC Generation Experiment Yields**
**Related to Figure 1 and Figure S3**
iBLC generation experiments over the course of this study with respect to initial iBLC observation and relative outcomes.

| LSM700 | Detector Gains | Hoechst | OCT4 | TROMA-I | | LSM880 | Detector Gains | Hoechst | OCT4 | TROMA-I |
|---|---|---|---|---|---|---|---|---|---|---|
| iBLC Control Setting | | 339 | 748 | 406 | | iBLC Control Setting | | 398 | 731 | 513 |
| Blastocyst-1 | | 363 | 491 | 540 | | Blastocyst-1 | | 356 | 502 | 537 |
| Blastocyst-2 | | 332 | 447 | 457 | | Blastocyst-2 | | 367 | 538 | 585 |
| Blastocyst-3 | | 375 | 462 | 515 | | Blastocyst-3 | | 363 | 601 | 604 |
| | | | | | | | | | | |
| **LSM700** | **Detector Gains** | **Hoechst** | **OCT4** | **TROMA-I** | | **LSM880** | **Detector Gains** | **Hoechst** | **OCT4** | **TROMA-I** |
| iBLC Control Setting | | 361 | 552 | 463 | | iBLC Control Setting | | 293 | 745 | 612 |
| Blastocyst-1 | | 384 | 414 | 503 | | Blastocyst-1 | | 344 | 634 | 630 |
| Blastocyst-2 | | 403 | 420 | 531 | | Blastocyst-2 | | 344 | 609 | 705 |
| Blastocyst-3 | | 415 | 443 | 557 | | Blastocyst-3 | | 354 | 561 | 619 |

**Table S2. iBLC vs BC Comparative Microscopy Gain Measurements**
**Related to Figure 4**

iBLC stained for DNA, OCT4, or TROMA-I detection are imaged on LSM700 and LSM880 microscopes (see Methods). Three BCs are stained the same as one iBLC and imaged with matching microscope settings to determine detector gains (see Methods). Higher gain numbers indicate fluorescence that was harder to detect and therefore likely in lower abundance.

**EB, mEpiSC Cluster, iBLC, and Control Embryo (BC)**
**Single Source and Co-Transfer Uterus Transfer Decidualization Experiments**

| Control Embryos Only | Control Embryos | n/a | Deciduae Observed | # above control | Control Decidualization Frequency |
|---|---|---|---|---|---|
| | 7 | 0 | 6 | 0 | 86% |
| | 7 | 0 | 0 | 0 | 0% |
| | 7 | 0 | 7 | 0 | 100% |
| | 7 | 0 | 3 | 0 | 43% |
| | 10 | 0 | 10 | 0 | 100% |
| | 10 | 0 | 10 | 0 | 100% |
| | 4 | 0 | 0 | 0 | 0% |
| | | | | | |
| **iBLCs Only** | **Control Embryos** | **iBLCs** | **Deciduae Observed** | **# above control** | **iBLC Decidualization Frequency** |
| | 0 | 10 | 0 | 0 | 0% |
| | 0 | 10 | 6 | **6** | **60%** |
| | 0 | 10 | 0 | 0 | 0% |
| | 0 | 10 | 0 | 0 | 0% |
| | 0 | 10 | 1 | **1** | **10%** |
| | 0 | 8 | 0 | 0 | 0% |
| | 0 | 10 | 2 | **2** | **20%** |
| | 0 | 11 | 0 | 0 | 0% |
| | 0 | 10 | 0 | 0 | 0% |
| | 0 | 10 | 0 | 0 | 0% |
| | 0 | 10 | 0 | 0 | 0% |
| | 0 | 10 | 1 | **1** | **10%** |
| | 0 | 10 | 0 | 0 | 0% |
| | 0 | 10 | 0 | 0 | 0% |
| | 0 | 10 | 0 | 0 | 0% |
| | | | | | |
| **iBLC + Control Co-Transfer** | **Control Embryos** | **iBLCs** | **Deciduae Observed** | **# above control** | **Control Decidualization Frequency *** |
| | 4 | 8 | 5 | **1** | **125%** |
| | 5 | 5 | 7 | **2** | **140%** |
| | 5 | 5 | 0 | 0 | 0% |
| | 5 | 5 | 4 | 0 | 80% |
| | 4 | 7 | 5 | **1** | **125%** |
| | 5 | 5 | 8 | **3** | **160%** |
| | 5 | 5 | 6 | **1** | **120%** |
| | 5 | 5 | 5 | 0 | 100% |
| | 5 | 6 | 4 | 0 | 80% |
| | 5 | 6 | 6 | **1** | **120%** |
| | 4 | 8 | 4 | 0 | 100% |
| | 4 | 9 | 0 | 0 | 0% |
| | 4 | 10 | 5 | **1** | **125%** |
| | 4 | 8 | 6 | **2** | **150%** |
| | 4 | 8 | 5 | **1** | **125%** |
| | 4 | 8 | 5 | **1** | **125%** |
| | 4 | 8 | 5 | **1** | **125%** |
| | 3 | 7 | 4 | **1** | **133%** |
| | 2 | 8 | 0 | 0 | 0% |
| | 4 | 8 | 7 | **3** | **175%** |

| | | | | | |
|---|---|---|---|---|---|
| | 4 | 7 | 3 | 0 | 75% |
| | 4 | 8 | 8 | **4** | **200%** |
| | 4 | 8 | 3 | 0 | 75% |
| | 4 | 8 | 3 | 0 | 75% |
| | 4 | 8 | 5 | **1** | **125%** |
| | 4 | 8 | 3 | 0 | 75% |
| | | | | | |
| **EB + Control Co-Transfer** | **Control Embryos** | **EB** | **Deciduae Observed** | **# above control** | **Control Decidualization Frequency *** |
| | 4 | 8 | 0 | 0 | 0% |
| | 4 | 7 | 0 | 0 | 0% |
| | | | | | |
| **EB Only** | **Control Embryos** | **EB** | **Deciduae Observed** | **# above control** | **EB Decidualization Frequency** |
| | 0 | 10 | 0 | 0 | 0% |
| | 0 | 7 | 0 | 0 | 0% |
| | 0 | 10 | 0 | 0 | 0% |
| | 0 | 10 | 0 | 0 | 0% |
| | | | | | |
| **mEpiSC Cluster + Control Co-Transfer** | **Control Embryos** | **mEpiSC Clusters** | **Deciduae Observed** | **# above control** | **Control Decidualization Frequency *** |
| | 4 | 8 | 2 | 0 | 50% |
| | 4 | 8 | 3 | 0 | 75% |
| | 4 | 8 | 4 | 0 | 100% |
| | 4 | 8 | 2 | 0 | 50% |
| | | | | | |
| **mEpiSC Cluster Only** | **Control Embryos** | **mEpiSC Clusters** | **Deciduae Observed** | **# above control** | **mEpiSC Decidualization Frequency** |
| | 0 | 10 | 0 | 0 | 0% |
| | 0 | 10 | 0 | 0 | 0% |
| | 0 | 10 | 0 | 0 | 0% |
| | 0 | 10 | 0 | 0 | 0% |

*Control Embryos are the positive control value. Calculations assume control embryo deciduae and maximal 100% result. Deciduae in excess of 100% control are **bold** and obviate iBLC contribution.

**Table S3. EB, mEpiSC cluster, iBLC, and BC Decidualization Experiments**
**Related to Figure 6**
Sterile-male bred pseudopregnant mice (PP2.5) surrogate transfer unit counts and subsequent dissected deciduae counts.

# SUPPLEMENTAL EXPERIMENTAL PROCEDURES

| REAGENT or RESOURCE | SOURCE | IDENTIFIER |
|---|---|---|
| **Antibodies** | | |
| Mouse anti-Mouse OCT4 (C-10) | Santa Cruz Biotech | sc-5279 |
| Rat anti-Mouse TROMA-I (KRT8) | DSHB | Troma-I |
| Mouse anti-Mouse PL-I | Santa Cruz Biotech | sc-376436 |
| Rabbit anti-Mouse TPBPA | Abcam | ab104401 |
| Mouse anti-Mouse YAP | Santa Cruz Biotech | sc-101199 |
| Rabbit anti-Mouse CDX2 | Abcam | ab76541 |
| Rabbit anti-Mouse CDX2 | Hitoshi Niwa Lab | |
| Mouse anti-Mouse NANOG | BD Pharmingen | 560259 |
| Mouse anti-Mouse GATA3 | Santa Cruz Biotech | sc-268 |
| Mouse anti-Mouse GATA4 (G-4) | Santa Cruz Biotech | sc-25310 |
| Goat anti-Mouse PDGFRa | RnD Systems | AF1062 |
| Goat anti-GATA6 (cross reactive with mouse) | RnD Systems | AF1700 |
| Donkey anti-Mouse Alexa Fluor 488 | Thermo Fisher | A-21202 |
| Donkey anti-Mouse Alexa Fluor 546 | Thermo Fisher | A-10036 |
| Donkey anti-Mouse Alexa Fluor 555 | Thermo Fisher | A-31570 |
| Donkey anti-Mouse Alexa Fluor 647 | Thermo Fisher | A-31571 |
| Donkey anti-Mouse Alexa Fluor 647 (preadsorbed) | Abcam | ab150111 |
| Donkey anti-Goat Alexa Fluor 647 | Thermo Fisher | A-21447 |
| Donkey anti-Rabbit Alexa Fluor 546 | Thermo Fisher | A-10040 |
| Donkey anti-Rat Alexa Fluor 647 | Jackson ImmunoRes. | 712-605-150 |
| Goat anti-Rat Alexa Fluor 555 | Thermo Fisher | A-21434 |
| Goat anti-Rat Alexa Fluor 647 | Thermo Fisher | A-21247 |
| Goat anti-Mouse Alexa Fluor 488 | Thermo Fisher | A-11029 |
| Goat anti-Mouse Alexa Fluor 546 | Thermo Fisher | A-11030 |
| Goat anti-Mouse Alexa Fluor 647 | Thermo Fisher | A-21236 |
| Goat anti-Rabbit Alexa Fluor 488 | Thermo Fisher | A-11008 |

| | | |
|---|---|---|
| Goat anti-Rabbit Alexa Fluor 488 (preadsorbed) | Abcam | ab150081 |
| | | |
| **Chemicals, Peptides, and Recombinant Proteins** | | |
| Recombinant BMP4 | RnD Systems | 314-BP-010 |
| Recombinant Activin A | RnD Systems | 338-AC-010 |
| Recombinant bFGF | Wako | 064-05381 |
| 2S-OMPT | Avanti Lipids | 857235P |
| SB431542 | Selleckchem | S1067 |
| ESGRO LIF | Millipore | ESG1106 |
| L-Ascorbic Acid 2-Phosphate | Sigma | A8960-5G |
| Fibronectin from Bovine Plasma Solution | Sigma | F1141-2MG |
| CHIR99021 | SelleckChem | S2924 |
| PD0325901 | SelleckChem | S1036 |
| DMEM/F12 Glutamax Medium | Life Technologies | 10565-018 |
| Neurobasal Medium | Life Technologies | 21103-049 |
| N-2 Supplement | Life Technologies | 17502-048 |
| B-27 Supplement | Life Technologies | 17504-044 |
| 100X Glutamax Supplement | Life Technologies | 35050-061 |
| 7.5% BSA Frac V | Life Technologies | 15260-037 |
| NDiff227 Medium | Clontech/Takara | Y40002 |
| 1000X 2-Mercaptoethanol | Life Technologies | 21985-023 |
| PBS (Ca/Mg free) | Life Technologies | 14190-094 |
| 100X Penicillin / Streptomycin | Thermo Fisher | 15140-122 |
| KnockOut DMEM | Thermo Fisher | 10829018 |
| KnockOut Serum Replacement | Thermo Fisher | 10828028 |
| MEM Non-Essential Amino Acids Solution (100X) | Thermo Fisher | 11140050 |
| iMatrix 511 | Nippi | 892011 |
| | | |
| **Experimental Models: Cell Lines** | | |
| XGFP mEpiSC (Female); Tg(CAG-EGFP)D4Nagy; 129X1/SvJ x 129S1/Sv)F1-Kitl | Azim Surani Lab | (Bao et al., 2009) |

| | | |
|---|---|---|
| XGFP mEpiSC (Female); Tg(CAG-EGFP)D4Nagy; 129X1/SvJ x 129S1/Sv)F1-Kitl; Piggybac *EOS::*mCherry (RFP) | This Paper | |
| XGFP mEpiSC (Female); Tg(CAG-EGFP)D4Nagy; 129X1/SvJ x 129S1/Sv)F1-Kitl; Piggybac *EOS::*DSRED (RFP) | This Paper | |
| XGFP mEpiSC (Female); Tg(CAG-EGFP)D4Nagy; 129X1/SvJ x 129S1/Sv)F1-Kitl; Piggybac *EOS::*D2-3xNLS-mCherry (D2nRFP) | This Paper | |
| XGFP mEpiSC (Female); Tg(CAG-EGFP)D4Nagy; 129X1/SvJ x 129S1/Sv)F1-Kitl; Piggybac *MERVL::*DSRED | This Paper | |
| XGFP mEpiSC (Female); Tg(CAG-EGFP)D4Nagy; 129X1/SvJ x 129S1/Sv)F1-Kitl; Piggybac *MERVL::*mCherry | This Paper | |
| mEpiSC (Female) | Satoshi Ohtsuka Lab | (Ohtsuka et al., 2012) |
| mEpiSC | Paul Tesar Lab | (Tesar et al., 2007) |
| mEpiSC, miRNA reporter GFP/RFP line | Robert Blelloch Lab | (Parchem et al., 2014) |
| | | |
| **Experimental Models: Organisms/Strains** | | |
| CD-1 (ICR) Surrogate Mice (Female) | RIKEN CDB Large | |
| CD-1 (ICR) Blastocysts (mixed gender) | RIKEN CDB Large | |
| R26-H2B-EGFP Blastocysts (mixed gender) | RIKEN CDB Large | CDB0238K |
| | | |
| **Oligonucleotides** | | |
| Taqman probe, Mouse Gapdh | Applied Biosystems | Mm99999915_g1 |
| Taqman probe, Mouse Pou5f1 (Oct4) | Applied Biosystems | Mm03053917_g1 |
| Taqman probe, Mouse Nanog | Applied Biosystems | Mm02019550_s1 |
| Taqman probe, Mouse Troma-I (Krt8) | Applied Biosystems | Mm04209403_g1 |
| Taqman probe, Mouse Atp1b1 | Applied Biosystems | Mm00437612_m1 |
| Taqman probe, Mouse Cdx2 | Applied Biosystems | Mm01212280_m1 |
| Taqman probe, Mouse Bmp4 | Applied Biosystems | Mm00432087_m1 |
| Taqman probe, Mouse Lifr | Applied Biosystems | Mm00442942_m1 |
| Taqman probe, Mouse Gata3 | Applied Biosystems | Mm00484683_m1 |
| Taqman probe, Mouse Prdm14 | Applied Biosystems | Mm01237814_m1 |
| Taqman probe, Mouse Prdm1 (Blimp1) | Applied Biosystems | Mm00476128_m1 |
| Taqman probe, Mouse Id1 | Applied Biosystems | Mm00775963_g1 |
| Taqman probe, Mouse Id2 | Applied Biosystems | Mm00711781_m1 |
| Taqman probe, Mouse Id3 | Applied Biosystems | Mm00492575_m1 |
| Taqman probe, Mouse Id4 | Applied Biosystems | Mm00499701_m1 |
| Taqman probe, Mouse Zscan4 | Applied Biosystems | Mm02581232_m1 |
| Taqman probe, Mouse Eomes | Applied Biosystems | Mm01351984_m1 |
| Taqman probe, Mouse Tdgf1 (Cripto) | Applied Biosystems | Mm03024051_g1 |
| Taqman probe, Mouse Cdh1 (Ecadherin) | Applied Biosystems | Mm01247357_m1 |
| Taqman probe, Mouse Gata4 | Applied Biosystems | Mm00484689_m1 |
| Taqman probe, Mouse Sox2 | Applied Biosystems | Mm03053810_s1 |
| Taqman probe, Mouse Sox17 | Applied Biosystems | Mm00488363_m1 |
| Taqman probe, Mouse Zfp42 (Rex1) | Applied Biosystems | Mm03053975_g1 |
| Taqman probe, Mouse Tcstv3 | Applied Biosystems | Mm02025498_s1 |

| | | |
|---|---|---|
| **Recombinant DNA** | | |
| 2C MERVL reporter DNA element (742bp) subcloned | Addgene | Plasmid #40281 |
| EOS reporter DNA element (907bp) subcloned | Addgene | Plasmid #21314 |
| Piggybac Transposon System | SBI | |
| | | |
| **Software and Algorithms** | | |
| Expression Suite Software V1.1 | Applied Biosystems | |
| Cluster 3.0 and Treeview 1.60 | Michael Eisen, Michiel de Hoon | http://bonsai.hgc.jp/~mdehoon/software/cluster/software.htm |
| Zeiss Zen Software | Zeiss | http://www.zeiss.com |
| FIJI / Image J | NIH | https://fiji.sc |
| GIMP 2.8 | GIMP Developers | https://www.gimp.org |
| Volocity 3D Visualisation | Perkin Elmer | |
| AVS Video Editor | AVS | http://www.avs4you.com |
| | | |
| **Other** | | |
| Ambion Nuclease Free Water | Thermo Fisher | AM9939 |
| Taqman Gene Expression Cells to CT Kit | Thermo Fisher | 4399002 |
| Taqman Gene Expression Mastermix | Thermo Fisher | 4369016 |
| Taqman Fast Universal PCR Mastermix (2x) | Thermo Fisher | 4352042 |
| TRIzol | Thermo Fisher | 15596026 |
| QIAzol | Qiagen | 79306 |
| Superscript Reverse Transcriptase III FS Kit | Thermo Fisher | 18080051 |
| Ambion RNASecure | Thermo Fisher | AM7010 |
| Tissue Tek OCT Compound | Fisher Scientific | 50-363-579 |
| Pierce 16% Formaldehyde (w/v) | Thermo Fisher | 28908 |
| Horse Serum, Heat Inactivated | Thermo Fisher | 26050070 |
| Polyvinylpyrrolidone | Sigma | P2307-100G |
| Fluorsave (Calbiochem) | Millipore | 345789 |
| Accutase | Millipore | SCR005 |
| Embryo Transfer Pipettes, 0.290-0.310mm | Vitrolife | 14319 |
| Hydrocell 3.5cm Low Attachment Dish | CellSeed | CS2005 |

| | | |
|---|---|---|
| QIAmp DNA Micro Kit | Qiagen | 56304 |
| Costar 24 Well Clear Flat Bottom Ultra Low Attachment Multiple Well Plates | Corning | 3473 |
| Falcon 6 Well Clear Flat Bottom TC-Treated Multiwell Cell Culture Plate | Corning | 353046 |
| Nunclon Sphera Round Bottom 96 Well Super Low Attachment Microplate | Thermo Fisher | 174925 |
| Zeiss PALM Adhesive Cap 500uL Tubes | Zeiss | 415190-9211-000 |
| | | |

**Contact for Reagent and Resource Sharing**
Further information and requests for reagents can be directed to Cody Kime (cody.kime@riken.jp). MTAs required.

**Method Details**
**iBLC/iBLC-PC Outgrowth Experiments**
6-well plates were coated with iMatrix511 and then plated with feeder cells and incubated overnight. The feeders were evenly plated and freshly prepared 2iLIF or CDM-FAXY was changed in at 1 mL/well from medias prepared as follows:

**2iLIF:** 200 mL CTSFES Basal Media + additional 1.2 mL 7.5% BSA Frac V Solution, 1000 units/mL ESGRO LIF, 3 µM CHIR99021, and 1 µM PD0325901, prepared fresh every 4 days.

**CDM-FAXY:** 200 mL of CTSFES Basal Media + 1.2 mL 7.5% BSA Frac V Solution, with supplements as published previously (Ohinata and Tsukiyama, 2014) except with 1:1000 2-ME in place of monothioglycerol.

iBLC and iBLC-PC were purified by embryo pipette and combined. The combined structures were pipetted against the bottom of the tube to break them up and then plated in the wells of 2iLIF or CDM-FAXY media, changed every other day. After one week, wells were replated in their respective medias on fresh feeders on 6-well plates coated with iMatrix511. 2iLIF cultures were then fed media daily with cell passage thereafter on iMatrix511 coated plates without feeders. CDM-FAXY cultures were fed every other day, replated once more onto iMatrix511 coated plates without feeders and then twice thereafter on fibronectin coated plates.

**Embryoid Body Formation Experiment**
*EB Medium ~100 mL:* [80 mL KnockOut DMEM, 20 mL KnockOut Serum Replacement, 1:1000 2-ME, 1 mL Non-Essential Amino Acids Solution, 1 mL Glutamax, 1:100 penicillin/streptomycin]; prepared fresh.

mEpiSC were prepared as single cells as in preparation for Naive Conversion or iBLC Generation until pelleted. The pellet was resuspended in 1 mL of EB Medium, and live cells were counted. Cells were plated at 100 µL/well in 96-Well Nunclon Sphera Super Low Attachment Microplates, at 500, 1000, or 2000 cells/well and incubated at 37 $^{0}$C. On Day 4, 100 µL of additional EB medium was added per well. EBs were collected on Day 8, and smaller sized and evenly formed EBs were sourced for IVF transfer into PP2.5 sterile-male bred pseudopregnant mice. When EBs were transferred to pseudopregnant mice, they were washed 3 times by transfer into separate drops of standard embryo-transfer medium.

**Mouse Decidua Dissection and Cryosections**
Surrogate mice were sacrificed humanely by standard protocol at E5.5–E9.5, as estimated by transfer timing at PP2.5. Mice were viewed from ventral side and the abdominal area was dissected to present the uterus horns to the fore and posterior of the mouse. Distinct deciduae were counted and noted on mouse cards and dissections were imaged with Sony Xperia 3 S0-01G. Deciduae selected for cryosection were dissected from uterine tissue to individual deciduae, washed in DPBS, and then fixed overnight in

paraformaldehyde at 4 $^0$C. Fixed deciduae were washed with PBS and then gradually desiccated with 30% Sucrose/PBS solution overnight at 4 $^0$C and then washed and placed in OCT Compound. Deciduae from one uterus horn were pooled into one sectioning mold, labeled, and stored at -80 $^0$C in OCT compound. OCT compound molds of deciduae were placed in the Microm HM560 microtome at -20 $^0$C and sections are cut at 10–30 µM thickness and placed on slide glass, dried for 1–2 hours under room temperature blown air, dried 1 hour at 37 $^0$C, then stored at -30 $^0$C in sealed slide containers until later use. Figure S5D sections were cut at 5 µM thickness.

**Hematoxylin and Eosin (H&E) Staining**

Previously prepared cryosections of deciduae were thawed from frozen slides and rinsed in PBS, stained with hematoxylin for 5 minutes, eosin for 2 minutes, and then washed with increasing mixed alcohol concentrations and then xylene before finalization in malinol with coverslips sealed by nail polish.

**Fluorescence Imaging and Confocal Microscopy**

Immunocytochemistry in Figure S1 A,B was carried out by fixation with paraformaldehyde and then blocking and staining in 5% BSA/PBS with mouse anti-mouse Nanog 1:200; then donkey anti-mouse Alexa Fluor 555 1:200, followed by Hoechst 33342 1:1000; imaged in PBS with Zeiss LSM 510 Confocal Microscope. Z-stack images from these samples were used for Video S1 by visualization in Volocity software, exported to video and labeled with AVS Video Editor which processed the 16:9 aspect ratio and reduced data size. Figure S1C was prepared using the same methods with 3 µg/mL of rat anti-mouse TROMA-I and mouse anti-mouse Nanog 1:200; then goat anti-rat Alexa Fluor 555 1:500 and donkey anti-mouse Alexa Fluor 647 (Thermo) 1:500, followed by Hoechst 33342 1:1000.

Live-cell XGFP fluorescence was imaged in Figure S2A Zeiss Z1 microscope.

DNA stain and imaging in Figure S3B were carried out by fixation with paraformaldehyde, permeabilization in 0.2% Triton X-100, and blocking and staining in 2% FBS/PBS; Hoechst 33342 1:2000, and imaged in 20% glycerol/PBS suspension slide with Olympus Confocal Microscope (CSU-X1).

Immunocytochemistry in Figure S1D, Figure 3A,B,C, Figure 4B,C,D,E, and Figure S3F was carried out by washing BCs or iBLCs or iBLC-PCs in 3 mg/mL polyvinylpyrrolidone in PBS, fixation with paraformaldehyde, permeabilization in 0.25% Triton X-100, and blocking and staining in 4% horse serum/PBS.

Figure S1D samples were stained as follows:

(top) 1:100 mouse anti-mouse GATA4 and 3.6 µg/mL rat anti-mouse TROMA-I; then 1:500 goat anti-mouse Alexa Fluor 546 and 1:500 goat anti-rat Alexa Fluor 647.

(mid) 1:100 mouse anti-mouse GATA4 and 2 µg/mL goat anti-mouse PDGFRa; then 1:500 donkey anti-mouse Alexa Fluor 546 and 1:500 donkey anti-goat Alexa Fluor 647.

(bottom) 1:100 mouse anti-mouse GATA4 and 2 µg/mL goat anti-mouse GATA6; then 1:500 donkey anti-mouse Alexa Fluor 546 and 1:500 donkey anti-goat Alexa Fluor 647.

Figure 3A,B,C samples were stained with 1:100 mouse anti-mouse YAP; then 1:500 goat anti-mouse Alexa Fluor 647.

Figure 4B samples were stained 1:100 mouse anti-mouse YAP and 1:100 rabbit anti-mouse CDX2(Abcam); then 1:500 goat anti-mouse Alexa Fluor 647 and 1:500 goat anti-rabbit Alexa Fluor 488 (Thermo).

Figure 4C samples were stained with 3.6 µg/mL rat anti-mouse TROMA-I and mouse anti-mouse GATA3 1:100; then goat anti-mouse Alexa Fluor 546 and 1:500 and goat anti-rat Alexa Fluor 647.

Figure 4D and Figure S3F samples were stained with 1:100 mouse anti-mouse GATA4 and 2 µg/mL goat anti-mouse PDGFRa; then 1:500 donkey anti-mouse Alexa Fluor 546 and 1:500 donkey anti-goat Alexa Fluor 647.

Figure 4E samples were stained with 3.6 µg/mL rat anti-mouse TROMA-I and mouse anti-mouse OCT4 1:200; then goat anti-mouse Alexa Fluor 488 and 1:500 and goat anti-rat Alexa Fluor 647.

All samples were followed by Hoechst 33342 stain 1:1000-2000 and imaged in 20% glycerol/PBS

suspension slide with Zeiss LSM 700 or 880 Confocal Microscopes. Samples were washed with blocking buffer ~3 times between fixing and staining. Figure S1D, Figure 4D and Figure S3F samples were imaged soon after placing in PBS suspension slide without glycerol.

IHC in Figure 7C was carried out by thawing previously cryosectioned deciduae slides, washing with PBS, permeabilization with 0.2% Triton X-100, and then blocking and staining in either 2% BSA/PBS or 4% horse serum/PBS with 1.8–9 µg/mL rat anti-mouse TROMA-I; then donkey anti-rat Alexa Fluor 647 1:250–500, followed by Hoechst 33342 1:2000, sealed in Fluorsave and imaged with Zeiss LSM 700 Confocal Microscope.

Immunocytochemistry in Figure S1E,F was prepared by fixation with paraformaldehyde, permeabilization in 0.25% Triton X-100, and blocking and staining in 4% horse serum/PBS. Antibodies were used in separate stains:

(Figure S1E) 1:100 mouse anti-mouse GATA4 and 2 µg/mL goat anti-mouse PDGFRa; then 1:500 donkey anti-mouse Alexa Fluor 546 and 1:500 donkey anti-goat Alexa Fluor 647.

(Figure S1F) 2 µg/mL goat anti-mouse GATA6; then 1:500 donkey anti-goat Alexa Fluor 647.

All staining was followed by Hoechst 33342 1:2000 and imaged with Zeiss LSM 700 Confocal Microscope. Samples were washed with blocking buffer ~3 times between fixing and staining stages.

Immunocytochemistry in Figure 5A was prepared by fixation with paraformaldehyde, permeabilization in 0.25% Triton X-100, and blocking and staining in 4% horse serum/PBS. Antibodies were used in separate stains:

(OCT4) 1:100 mouse anti-mouse OCT4; then 1:500 goat anti-mouse Alexa Fluor 647.

(NANOG) 1:100 mouse anti-mouse NANOG, then 1:500 goat anti-mouse Alexa Fluor 647.

(YAP) 1:100 mouse anti-mouse YAP, then 1:500 goat anti-mouse Alexa Fluor 647.

All staining was followed by Hoechst 33342 1:2000 and imaged with Zeiss LSM 700 Confocal Microscope. Samples were washed with blocking buffer ~3 times between fixing and staining stages.

Immunocytochemistry of TE-like cells in Figure 5C was prepared by fixation with paraformaldehyde, permeabilization in 0.2% Triton X-100, and blocking and staining in 4% horse serum/PBS with rabbit anti-mouse CDX2 (gift from Hitoshi Niwa) 1:1000; then goat anti-rabbit Alexa Fluor 488 (Thermo) 1:500, followed by Hoechst 33342 1:2000 and imaged in PBS with Zeiss LSM 700 Confocal Microscope. Sample was washed with blocking buffer ~3 times between fixing and staining.

IHC in Figure S5D was carried out by thawing previously cryosectioned deciduae slides, air dried, washing with PBS, permeabilization with 0.1% Triton X-100, and then blocking in 2.5% skim milk for 30 min. The blocked sections were stained separately as follows:

(PL-I) 1:100 mouse anti-mouse PL-I; then 1:1000 donkey anti-mouse Alexa Fluor 647 (Abcam).

(TPBPA) 1:100 rabbit anti-mouse TPBPA; then 1:1000 goat anti-rabbit Alexa Fluor 488 (Abcam).

All staining was followed by DAPI for nuclear DNA visualization and imaged on both the LSM 700 Confocal Microscope and Keyence BZ-X700. Samples were washed with blocking buffer ~3 times between fixing and staining stages. Negative control samples were stained without primary antibodies and with the two secondary antibodies combined. Fluorescent signals were pseudo-colored red for clarity.

Live cell RFP and GFP fluorescence was imaged in Figure 2A,B,C, Figure 4F, Figure S2C, Figure S3D,G, Figure S4A,B with a Olympus IX71 Microscope.

Immunocytochemistry in Figure S4B was prepared by fixation with paraformaldehyde, permeabilization in 0.25% Triton X-100, and blocking and staining in 4% horse serum/PBS. Antibodies were used in separate stains:

1:100 mouse anti-mouse PL-I; then 1:500 donkey anti-mouse Alexa Fluor 488.

1:100 rabbit anti-mouse TPBPA, then 1:500 donkey anti-rabbit Alexa Fluor 546.

All staining was followed by Hoechst 33342 1:2000 and imaged with Zeiss LSM 700 Confocal Microscope. Samples were washed with blocking buffer ~3 times between fixing and staining stages.

**Comparative Microscopy**

Zeiss LSM700 and LSM880 confocal microscopes were used as indicated in Table S2 for qualitative comparative microscopy as follows: For each iBLC sample, channel laser intensities, pinhole, and objective were selected to produce a clear image. The channel gains were determined manually by setting each channel with range indicators and increasing channel detector gains until few target pixels saturated the signal, and then the image was captured. For comparison to each of those iBLC samples, three BCs prepared with identical methods were imaged with the same microscope, laser intensity, pinhole, and objective settings as the compared iBLC image. The channel gains were then adjusted manually by the same method of using the range indicator setting and increasing the gain until few target pixels saturated the signal, and then the image was captured.

**Light Microscopy**

Bright field and phase contrast microscopy were carried out on several microscope models. When accompanied by or prepared as composite in fluorescent images, the same microscope was used. Figure S3A images were taken with Olympus CKX41 Microscope. Figure 1B,C, Figure 2A,B,C,G, Figure 4F, Figure 5C (left panel), Figure S2C, Figure S3D,G, FigureS4A,B,C were taken with Olympus IX71 Microscope.

H&E Stained cryosection slides in Figure 7A,B, Figure S5A,B,C, were imaged with Olympus IX71 Microscope.

Sony Xperia 3 S0-01G was used for Figure 6B.

Zeiss Laser Palm Microbeam was used for imaging Figure S5A(right panels).

**Laser Capture Microdissection and gDNA PCR**

Unique primers for hygromycin resistance transgene were designed using NCBI Primer Blast web software and optimal primers were selected. Jackson Labs (JAX) universal mouse genomic DNA primers were also used for control PCR. H&E stained cryosection samples of interest were prepared using standard slide cover removal techniques and then automated LCM with the Zeiss PALM Microbeam with close cut parameters. Selected tissues were collected with adhesive cap, 500 µL tubes. Genomic DNA was purified from collected tissues using the Zeiss PALM Protocols DNA Handling manual page 21 with a QIAmp DNA Micro Kit, eluting in 20 µL of nuclease free water. Genomic DNA purified from recombinant DNA integrated mEpiSC was used for positive control. 5 µL of purified sample was used in 25 µL PCR reactions with touchdown thermocycling using the following DNA oligonucleotide primers:

JAX Universal Mouse Forward: CTAGGCCACAGAATTGAAAGATCT
JAX Universal Mouse Reverse: GTAGGTGGAAATTCTAGCATCATCC
HygR Primer Set 2 Forward: GCTCAGGCACTGGATGAACT
HygR Primer Set 2 Reverse: CAGCCAGTTCTGGGTGTCTT

12.5 µL of PCR reactions were run in agarose gel electrophoresis and stained with ethidium bromide and remaining PCR sample was stocked as preamplified DNA. Samples used in Figure 6D were prepared by reamplification of 1:200 diluted preamplified DNA using target primer sets; 12.5 µL of that secondary reamplified reaction was run in 2.5% agarose gel electrophoresis.

**Quantification and Statistical Analysis**

**qRT-PCR Experiments**

For Figure 2E and Figure 4A: 3 BCs, 6 iBLCs, and 3 mEpiSC colonies were isolated with unique embryo pipettes and washed with CMF-DPBS and carried through standard Ambion Cells-to-CT protocol including optional DNAse I treatment. 50 µL of sample lysate was used for a 125 µL reverse transcription reaction, then diluted to 140 µL with nuclease free water. qRT-PCR was prepared for each sample in duplicate with TaqMan probes using 4 µL of sample cDNA in 20 µL reactions using TaqMan Gene Expression Mastermix. Detection was prepared on StepOne Plus under standard cycling conditions with *Gapdh* samples on each plate. Plate data was analyzed with Applied Biosystems Expression Suite v1.1. Figure S3E experiments were performed similarly, except using earlier stage iBLCs and BCs, and diluting 113 µL

of the reverse transcription reaction product with 40 µL of nuclease free water to ensure enough sample overage for qRT-PCR.

For Figure 2D: Three biological replicates of iBLC system induction experiments were conducted and then clusters that were possible iBLC-PC were collected on Day 6 and pooled based on the presence or absence of *MERVL::*RFP expression using fluorescence microscopy and embryo pipette. For each biological replicate, approximately 10 clusters were collected for each pool sample, then washed with CMF-DPBS and carried through standard Ambion Cells-to-CT protocol including optional DNAse I treatment. 50 µL of sample lysate was used for a 125 µL reverse transcription reaction, then diluted to 200 µL with nuclease free water. qRT-PCR was prepared for each sample in triplicate with TaqMan probes using 1 µL of sample cDNA in 20 µL reactions using TaqMan Gene Expression Mastermix. Detection was prepared on StepOne Plus under standard cycling conditions with *Gapdh* samples on each plate. Plate data was analyzed with Applied Biosystems Expression Suite v1.1 and expression data was visualized in Microsoft Excel. One control mEpiSC sample was prepared from approximately 2,000 cells, and two other control mEpiSC samples were collected by gently digesting mEpiSC culture and scraping colonies to float in CMF-DPBS and handled similar to iBLC-PC handling, and all were carried through standard Ambion Cells-to-CT kit sampling following the same methods. mEpiSC cDNA was diluted 1/10 before use in the same detection methods to bring *Gapdh* levels and templates closer to iBLC-PC sample levels.

For Figure 2F: Three biological replicate experiments of iBLC generation plates of *Prdm14* KD and control cell cultures on Day 6 were washed gently with PBS then total RNA was prepared with QIAzol standard techniques finalized in Ambion Nuclease Free Water. cDNA was prepared from total RNA using Superscript Reverse Transcriptase III FS Kit with Random Hexamers protocol and diluted with nuclease free water. qRT-PCR was carried out in 20 µL reactions with 2 µL of cDNA of each sample in triplicate for all TaqMan probes with standard fast reaction protocols in TaqMan Universal Fast Mastermix on StepOne Plus. Plate data was analyzed with Applied Biosystems Expression Suite v1.1 and expression data was visualized in Microsoft Excel.

For Figure 5B: iBLC/iBLC-PC derived outgrowths in 2iLIF media were cultured and passaged as neat colonies. C57BL/6N mouse ESCs were cultured similarly in 2iLIF media for positive control, and XGFP mEpiSC were cultured in MCM for negative control. Three biological replicates of each culture were sourced for total RNA via QIAzol purification methods and finalized in Ambion Nuclease Free Water. cDNA was prepared from total RNA using Superscript Reverse Transcriptase III FS Kit with Random Hexamers protocol and diluted with nuclease free water. qRT-PCR was carried out in 20 µL reactions with 2 µL of cDNA of each sample in triplicate for all TaqMan probes with standard fast reaction protocols in TaqMan Universal Fast Mastermix on StepOne Plus. Plate data was analyzed with Applied Biosystems Expression Suite v1.1 and expression data was visualized in Microsoft Excel.

For Figure S2B: Naive conversion and control cell cultures were washed with PBS then total RNA was prepared with TRIzol standard techniques and finalized in Ambion RNAsecure. cDNA was prepared from total RNAs using Superscript Reverse Transcriptase III FS Kit with Random Hexamers protocol. qRT-PCR was prepared for each sample in triplicate with standard fast reaction protocols in TaqMan Universal Fast Mastermix for 10ul reactions with TaqMan probes in 384W plate and run on Applied Biosystems 7900HT. Plate data was analyzed with SDS software and expression data was visualized in Microsoft Excel.

**Data Availability**

The data generated or analyzed in the current study are available from the corresponding author on reasonable request.

# SUPPLEMENTAL DISCUSSION

This study showed that post-implantation primed state mammalian PSCs can be induced by defined conditions into small *MERVL::*RFP+ clusters that polarize and self-organize emergent differentiation to form 3D cysts with features of BCs that can implant with some growth *in utero*. In previous work of mouse PSC-derived oogenesis, rare BC-like structures from 40+ day long-term differentiation experiments were briefly described (Hübner et al., 2003). However, isogenic PSCs have not previously demonstrated this range of early embryonic animal development characteristics in transplanted surrogates without donor cells or chimerism for support (Macfarlan et al., 2012; Yang et al., 2017b). Hereafter we consider how to improve upon the iBLC system.

*SMAD and Pluripotency in Conversion*

The insufficient pluripotency in iBLCs are in stark contrast to what we observed during the hemisphere formation experiments where naive pluripotency was robustly established (Kime et al., 2016). In that study, BMP4 signaling with LIF and ascorbic acid had greatly increased *Prdm14* expression during conversion of mEpiSCs to the naive state (Kime et al., 2016); but we also measured the induction of Prdm1 (Blimp1) and Id gene mRNAs, shown herein. BMP4 can replace serum in naive PSC culture by inducing Id genes toward self-renewal (Ying et al., 2003). BMP signaling and critical Prdm and Id family genes are shared among germ cell development and cleavage through pre-implantation embryonic development (Hiller et al., 2010; Tang et al., 2010; Wu et al., 2016; Yamaji et al., 2008; Yang et al., 2017a; Ying et al., 2003).

One considerable difference between naive conversion and iBLC generation is the SMAD2/3 signaling inhibitor SB which may induce BMP expression. SB may be necessary to generate iBLCs although SMAD2-specific inhibition induces TE and germ cell differentiation while suppressing pluripotency expression via Nanog inhibition (Chen et al., 2012; Sakaki-Yumoto et al., 2013). We anticipate that SMAD2 and/or SMAD3 signaling inhibition may require further adjustment to achieve sufficient potency from iBLCs and note that SB concentration was mEpiSC line specific.

*iBLC-PC Characteristics*

iBLC-PC YAP localization reflects non-polarized cells compacting and polarizing with key characteristics of early embryos; the intermediate MERVL and 2C gene expression strengthens that prospect. Signaling inputs of this system were influenced from developmental cues of embryogenesis (Cha et al., 2012), and our synthetic LPA (OMPT) may be helpful since LPA treated BCs exhibit enhanced embryogenesis via YAP *in vitro* and *in utero* (Yu et al., 2016).

*Prdm14* KD revealed an unknown pivotal role for Prdm14 in this system. *Prdm14* was greatly enriched prior to LIF supplementation (data not shown), which contrasts with conventional roles of LIF in ESC pluripotency (Ying et al., 2003). Taken with SMAD2/3 signaling inhibition we speculate that Phase 1 induced *Prdm14* may involve germ cell programming mechanisms. Prdm14 is a transcription factor that is both powerful and unclear: reported to be dispensable in BCs yet serves as a major epigenetic regulator in the 2C cleavage stage to possibly direct lineage commitment in the emerging BC (Burton et al., 2013; Luna-Zurita and Bruneau, 2013; Yamaji et al., 2008). Prdm14 is involved in dynamic biological events that accompany epigenetic reprogramming, such as PGC specification, X chromosome reactivation, and conversion from primed to naive state pluripotency (Gillich et al., 2012; Kime et al., 2016; Payer et al., 2013; Yamaji et al., 2008). *Prdm14* KD cells proceeded typically for several days until iBLC-PCs aborted among drastically reduced *Prdm14* and when iBLC-PCs should begin polarizing into iBLCs. Given that iBLC-PC loci and iBLC-PCs expressed the MERVL reporter that reflects the endogenous 2C gene expression, one can expect that *Prdm14* KD reduced 2C gene expressions. However, unexpectedly, this was not always the case and Prdm14 may have only been important for the iBLC system after that stage. How Prdm14 is involved in iBLC production and embryogenesis warrants further investigation.

Phase1 conditions resemble germ cell induction, and the germ line prepares a totipotent genome that is not yet activated epigenetically (Seydoux and Braun, 2006). Since iBLCs share many bi-directional features of BCs, which come from totipotent cells, the 2C ZGA mechanisms suggested by the concurrent MERVL activation and 2C gene expression may play a role (Wu et al., 2017). Supporting this notion, we observed the compacting iBLC-PC originating loci with concurrent *MERVL::*RFP+ cells with blastomere-like size and morphology. Previous studies of MERVL-enriched PSCs had touched upon totipotent hallmarks, ZGA, and 2C-like expression, yet such cells lacked clear differences from ESCs (Blaschke et al., 2013; Ishiuchi et al., 2015; Macfarlan et al., 2012). Several reports found ESC colonies have rare (~1%)

transient MERVL+ cells that return to the ESC state, yet iBLC experiments induced iBLC-PC loci and iBLC-PC that activated *MERVL::*RFP simultaneously and with relatively consistent sustained expression. Therefore, cells in iBLC experiments may transit a unique 2C-like metastate.

Enriched *Atp1b1* in isolated iBLCs was remarkable because embryos activate *Atp1b1* in the cleavage stage to act in cell junctions during compaction and as a Na+/K+ ATPase pump subunit to fill the blastocoel (Hamatani et al., 2004; Madan et al., 2007; Stephenson et al., 2010). iBLCs also activated *Zfp42* (Rex1) and *Zscan4*, which are also cleavage stage-induced genes with different roles in pluripotent cells. Moreover, Zfp42 (Rex1) may negatively regulate 2C-related gene expression (Schoorlemmer et al., 2014), yet the iBLC/iBLC-PC-derived ESC-like cells had elevated both *Zfp42* (Rex1) and *Zscan4* when compared to ESCs.

From these observations we anticipate that a thorough molecular elucidation of iBLC generation may improve upon MERVL/2C stability and/or iBLC with full BC functionality.

*iBLC Molecular Issues*

CDX2 is preferentially upregulated around the 8C stage of embryos and localizes in nuclei in outer cells to establish the TE lineage in collaboration with GATA3 (Home et al., 2009; Ralston and Rossant, 2008; Ralston et al., 2010; Strumpf et al., 2005). CDX2-deficient BCs cannot implant in the uterus yet retain pluripotent cells (Meissner and Jaenisch, 2006). Like BCs, iBLCs exhibit a CDX2+, TROMA-I+ and nuclear-enriched YAP outer layer with a blastocoel-like cavity and implanted *in utero*, suggesting establishment of some functional TE-like property in iBLCs.

After implantation the iBLC TROMA-I+ cells invaded the uterus to decidua reaction and grew toward different morphologies and markers depending on their positions in the embryonic cavity. Post-implantation proliferation of trophoblast progeny depends on ICM-derived tissues, suggesting help from the putative iBLC ICM-like mass (Gardner and Johnson, 1972, 1975; Rossant and Ofer, 1977; Simmons and Cross, 2005). Furthermore, the iBLC ICM-like mass was observed expressing the *EOS* reporter and OCT4 features of pluripotency and had nuclear-excluded YAP and downregulated both TROMA-I and CDX2. These data are particularly important because the exclusion of nuclear YAP is a characteristic of pluripotent cells in the ICM of BCs that is critically different from *in vitro* cultured mouse pluripotent ESCs that have nuclear-enriched YAP (Tamm et al., 2011). We speculate that the iBLC ICM-like mass became the TROMA-I- cells central to TROMA-I+ cells observed in cryosections as those regions had similar H&E stain characteristics to embryonic cells seen in proximal sections.

Further, PrE hypoblast-like characteristics, judged by GATA4, GATA6 and PDGFRa expressions and relative cell positioning, were evident in BC-like hemispheres but less distinct in iBLCs. However, GATA4 and PDGFRa were expressed in early iBLCs as with early BCs. In addition, curiously, we could see close similarity in collective formation of GATA4+ cells both in very late iBLCs and hatching BCs. Thus, we speculate that a PrE specification and hypoblast formation program are partially installed in iBLCs. Because hypoblast formation depends on emergence of naive pluripotent state in the ICM (Silva et al., 2009), observation of the hypoblast-like structure further support existence of the putative ICM in iBLCs. Collectively, we consider that iBLCs exhibit some features of all of three late BC lineages, albeit less distinct.

It is unclear which molecular issues fundamentally characterize iBLC imperfections. In early iBLCs, GATA3 and YAP were nearly properly expressed and localized while CDX2 was poorly regulated when compared to BCs. iBLC outer cells mostly retained cytosolic CDX2, and CDX2 was weakly downregulated in the iBLC putative ICM. OCT4 is crucial for pluripotency in BCs (Niwa et al., 2000) and was low in iBLCs although we could establish ESC-like cells in naive PSC derivation conditions. Given the complete downregulation of CDX2 is required for OCT4 activation to establish the ICM (Niwa et al., 2005), the poor establishment of pluripotency and hypoblast in iBLCs may stem from the poor regulation of CDX2 as described above. CDX2 dysregulation may be a diverging event for iBLCs and correcting CDX2 regulatory pathways could be key to obtain fully functional iBLCs.

*Concluding Remarks*

Until recently, only BCs or trophoblasts (Gardner and Johnson, 1972), chimeric assembly thereof, or specific melanoma cells were reported to induce deciduae in sterile-male bred pseudopregnant mice (Wilson, 1963). Recent studies combining TSC and ESC populations have reinforced previously described technologies to further elucidate the interdependence and complementation of the ExEm and Em lineages while highlighting the limitations of differentiated cells (Buhl et al., 2009; Gardner and Johnson, 1972;

Harrison et al., 2017; Rivron et al., 2018).

Adjusting the iBLC system to produce isogenic animals requires *in toto* potential from PSCs. For now, we provide evidence that isogenic PSC culture may intersect a 2C-like expression program with emergent polarization to self-organize the 3D architecture and cellular materials resembling BCs with implantation-competence. Generation of iBLCs requires stringent PSC preparation and iBLC purification, yet centers on 1 week of simple defined-media changes. Thus, we envision that the iBLC system may readily contribute to better understanding pluripotency, totipotency, embryogenesis, and related emergent fields.

# SUPPLEMENTAL REFERENCES

Blaschke, K., Ebata, K.T., Karimi, M.M., Zepeda-Martínez, J.A., Goyal, P., Mahapatra, S., Tam, A., Laird, D.J., Hirst, M., Rao, A., et al. (2013). Vitamin C induces Tet-dependent DNA demethylation and a blastocyst-like state in ES cells. Nature *500*, 222–226.

Buhl, S., Egert, A., Schorle, H., and Woynecki, T. (2009). Induced blastocyst-like structures, methods of production and uses of the same, EP2088191A1.

Burton, A., Muller, J., Tu, S., Padilla-Longoria, P., Guccione, E., and Torres-Padilla, M.-E. (2013). Single-Cell Profiling of Epigenetic Modifiers Identifies PRDM14 as an Inducer of Cell Fate in the Mammalian Embryo. Cell Rep. *5*, 687–701.

Cha, J., Sun, X., and Dey, S.K. (2012). Mechanisms of implantation: strategies for successful pregnancy. Nat. Med. *18*, 1754–1767.

Chen, W., Jia, W., Wang, K., Zhou, Q., Leng, Y., Duan, T., and Kang, J. (2012). Retinoic acid regulates germ cell differentiation in mouse embryonic stem cells through a Smad-dependent pathway. Biochem. Biophys. Res. Commun. *418*, 571–577.

Gardner, R.L., and Johnson, M.H. (1972). An investigation of inner cell mass and trophoblast tissues following their isolation from the mouse blastocyst. Development *28*, 279–312.

Gardner, R.L., and Johnson, M.H. (1975). Investigation of cellular interaction and deployment in the early mammalian embryo using interspecific chimaeras between the rat and mouse. Ciba Found. Symp. *0*, 183–200.

Gillich, A., Bao, S., Grabole, N., Hayashi, K., Trotter, M.W.B., Pasque, V., Magnúsdóttir, E., and Surani, M.A. (2012). Epiblast Stem Cell-Based System Reveals Reprogramming Synergy of Germline Factors. Cell Stem Cell *10*, 425–439.

Hamatani, T., Carter, M.G., Sharov, A.A., and Ko, M.S.H. (2004). Dynamics of Global Gene Expression Changes during Mouse Preimplantation Development. Dev. Cell *6*, 117–131.

Harrison, S.E., Sozen, B., Christodoulou, N., Kyprianou, C., and Zernicka-Goetz, M. (2017). Assembly of embryonic and extraembryonic stem cells to mimic embryogenesis in vitro. Science *356*, eaal1810.

Hiller, M., Liu, C., Blumenthal, P.D., Gearhart, J.D., and Kerr, C.L. (2010). Bone Morphogenetic Protein 4 Mediates Human Embryonic Germ Cell Derivation. Stem Cells Dev. *20*, 351–361.

Home, P., Ray, S., Dutta, D., Bronshteyn, I., Larson, M., and Paul, S. (2009). GATA3 is selectively expressed in the trophectoderm of peri-implantation embryo and directly regulates Cdx2 gene expression. J. Biol. Chem. jbc.M109.016840.

Hübner, K., Fuhrmann, G., Christenson, L.K., Kehler, J., Reinbold, R., Fuente, R.D.L., Wood, J., Strauss, J.F., Boiani, M., and Schöler, H.R. (2003). Derivation of Oocytes from Mouse Embryonic Stem Cells. Science *300*, 1251–1256.

Ishiuchi, T., Enriquez-Gasca, R., Mizutani, E., Bošković, A., Ziegler-Birling, C., Rodriguez-Terrones, D., Wakayama, T., Vaquerizas, J.M., and Torres-Padilla, M.-E. (2015). Early embryonic-like cells are induced by downregulating replication-dependent chromatin assembly. Nat. Struct. Mol. Biol. *9*, 662-71.

Kime, C., Sakaki-Yumoto, M., Goodrich, L., Hayashi, Y., Sami, S., Derynck, R., Asahi, M., Panning, B., Yamanaka, S., and Tomoda, K., (2016). Autotaxin-mediated lipid signaling intersects with LIF and BMP signaling to promote the naive pluripotency transcription factor program. Proc. Natl. Acad. Sci. *113*, 12478–12483.

Luna-Zurita, L., and Bruneau, B.G. (2013). Chromatin modulators as facilitating factors in cellular reprogramming. Curr. Opin. Genet. Dev. *23*, 556–561.

Macfarlan, T.S., Gifford, W.D., Driscoll, S., Lettieri, K., Rowe, H.M., Bonanomi, D., Firth, A., Singer, O., Trono, D., and Pfaff, S.L. (2012). Embryonic stem cell potency fluctuates with endogenous retrovirus activity. Nature *487*, 57–63.

Madan, P., Rose, K., and Watson, A.J. (2007). Na/K-ATPase β1 Subunit Expression Is Required for Blastocyst Formation and Normal Assembly of Trophectoderm Tight Junction-associated Proteins. J. Biol. Chem. *282*, 12127–12134.

Meissner, A., and Jaenisch, R. (2006). Generation of nuclear transfer-derived pluripotent ES cells from cloned Cdx2-deficient blastocysts. Nature *439*, 212–215.

Niwa, H., Miyazaki, J., and Smith, A.G. (2000). Quantitative expression of Oct-3/4 defines differentiation, dedifferentiation or self-renewal of ES cells. Nat. Genet. *24*, 372–376.

Niwa, H., Toyooka, Y., Shimosato, D., Strumpf, D., Takahashi, K., Yagi, R., and Rossant, J. (2005). Interaction between Oct3/4 and Cdx2 Determines Trophectoderm Differentiation. Cell 123, 917–929.

Payer, B., Rosenberg, M., Yamaji, M., Yabuta, Y., Koyanagi-Aoi, M., Hayashi, K., Yamanaka, S., Saitou, M., and Lee, J.T. (2013). Tsix RNA and the Germline Factor, PRDM14, Link X Reactivation and Stem Cell Reprogramming. Mol. Cell *52*, 805–818.

Ralston, A., and Rossant, J. (2008). Cdx2 acts downstream of cell polarization to cell-autonomously promote trophectoderm fate in the early mouse embryo. Dev. Biol. *313*, 614–629.

Ralston, A., Cox, B.J., Nishioka, N., Sasaki, H., Chea, E., Rugg-Gunn, P., Guo, G., Robson, P., Draper, J.S., and Rossant, J. (2010). Gata3 regulates trophoblast development downstream of Tead4 and in parallel to Cdx2. Development *137*, 395–403.

Rivron, N.C., Frias-Aldeguer, J., Vrij, E.J., Boisset, J.-C., Korving, J., Vivié, J., Truckenmüller, R.K., Oudenaarden, A. van, Blitterswijk, C.A. van, and Geijsen, N. (2018). Blastocyst-like structures generated solely from stem cells. Nature *557*, 106–111.

Rossant, J., and Ofer, L. (1977). Properties of extra-embryonic ectoderm isolated from postimplantation mouse embryos. Development *39*, 183–194.

Sakaki-Yumoto, M., Liu, J., Ramalho-Santos, M., Yoshida, N., and Derynck, R. (2013). Smad2 Is Essential for Maintenance of the Human and Mouse Primed Pluripotent Stem Cell State. J. Biol. Chem. *288*, 18546–18560.

Schoorlemmer, J., Pérez-Palacios, R., Climent, M., Guallar, D., and Muniesa, P. (2014). Regulation of Mouse Retroelement MuERV-L/MERVL Expression by REX1 and Epigenetic Control of Stem Cell Potency. Front. Oncol. *4*.

Seydoux, G., and Braun, R.E. (2006). Pathway to Totipotency: Lessons from Germ Cells. Cell *127*, 891–904.

Silva, J., Nichols, J., Theunissen, T.W., Guo, G., van Oosten, A.L., Barrandon, O., Wray, J., Yamanaka, S., Chambers, I., and Smith, A. (2009). Nanog Is the Gateway to the Pluripotent Ground State. Cell 138, 722–737.

Simmons, D.G., and Cross, J.C. (2005). Determinants of trophoblast lineage and cell subtype specification in the mouse placenta. Dev. Biol. *284*, 12–24.

Stephenson, R.O., Yamanaka, Y., and Rossant, J. (2010). Disorganized epithelial polarity and excess trophectoderm cell fate in preimplantation embryos lacking E-cadherin. Development *137*, 3383–3391.

Strumpf, D., Mao, C.-A., Yamanaka, Y., Ralston, A., Chawengsaksophak, K., Beck, F., and Rossant, J. (2005). Cdx2 is required for correct cell fate specification and differentiation of trophectoderm in the mouse blastocyst. Development *132*, 2093–2102.

Tamm, C., Böwer, N., and Annerén, C. (2011). Regulation of mouse embryonic stem cell self-renewal by a Yes–YAP–TEAD2 signaling pathway downstream of LIF. J Cell Sci *124*, 1136–1144.

Tang, F., Barbacioru, C., Bao, S., Lee, C., Nordman, E., Wang, X., Lao, K., and Surani, M.A. (2010). Tracing the Derivation of Embryonic Stem Cells from the Inner Cell Mass by Single-Cell RNA-Seq Analysis. Cell Stem Cell *6*, 468–478.

Wilson, I.B. (1963). A Tumour Tissue Analogue of the Implanting Mouse Embryo*. Proc. Zool. Soc. Lond. *141*, 137–151.

Wu, G., Lei, L., and Schöler, H.R. (2017). Totipotency in the mouse. J. Mol. Med. 1–8.

Wu, J., Huang, B., Chen, H., Yin, Q., Liu, Y., Xiang, Y., Zhang, B., Liu, B., Wang, Q., Xia, W., et al. (2016). The landscape of accessible chromatin in mammalian preimplantation embryos. Nature *534*, 652-657.

Yamaji, M., Seki, Y., Kurimoto, K., Yabuta, Y., Yuasa, M., Shigeta, M., Yamanaka, K., Ohinata, Y., and Saitou, M. (2008). Critical function of Prdm14 for the establishment of the germ cell lineage in mice. Nat. Genet. *40*, 1016–1022.

Yang, S., Yuan, Q., Niu, M., Hou, J., Zhu, Z., Sun, M., Li, Z., and He, Z. (2017a). BMP4 promotes mouse iPS cell differentiation to male germ cells via Smad1/5, Gata4, Id1 and Id2. Reproduction *153*, 211–220.

Yang, Y., Liu, B., Xu, J., Wang, J., Wu, J., Shi, C., Xu, Y., Dong, J., Wang, C., Lai, W., et al. (2017b). Derivation of Pluripotent Stem Cells with In Vivo Embryonic and Extraembryonic Potency. Cell *169*, 243-257.e25.

Ying, Q.-L., Nichols, J., Chambers, I., and Smith, A. (2003). BMP Induction of Id Proteins Suppresses Differentiation and Sustains Embryonic Stem Cell Self-Renewal in Collaboration with STAT3. Cell *115*, 281–292.

Yu, C., Ji, S.-Y., Dang, Y.-J., Sha, Q.-Q., Yuan, Y.-F., Zhou, J.-J., Yan, L.-Y., Qiao, J., Tang, F., and Fan, H.-Y. (2016). Oocyte-expressed yes-associated protein is a key activator of the early zygotic genome in mouse. Cell Res. *26*, 275–287.